Study on Mechanism and Kinetics of Key Reactions in Gasification of Lignite

崔, 哲溶

Studies on Mechanism and Kinetics of Key Reactions in Gasification of Lignite

by

Cheolyong Choi

(2019)

Department of Applied Science for Electronics and Materials

Interdisciplinary Graduate School of Engineering Sciences

Kyushu University, Japan

Contents

Chapter 1

General Introduction

1.1. Background

Gasification is a process that utilizes carbonaceous resources including not only fossil fuels but also various carbonaceous resources such as biomass and organic waste, taking advantage of low environmental impact and flexibility of both feedstock and product. The flexibility arises from a common form of gasified products, i.e. syngas composed mainly of H_2 and CO, regardless of the resources. For instance, gasification of coal is applied for power generation with lower emissions compared to conventional pulverized coal combustion and is also applicable to production of liquid fuel and chemicals, mainly produced by petrochemical process, as well as substitute natural gas depending on downstream configurations. Further, two or more products can be potentially produced at the same time or by switching the modes in a co-production (or poly-generation) system with high efficiency through integration of

thermal and chemical energy [1-10]. Gasification is thus expected to play an important role in the future industries.

Utilization of coal, of which price is inexpensive and stable, to the gasification is regarded as an important option in terms of energy security particularly for countries importing the majority of primary energy resources due to large fluctuation in the prices of crude oil and natural gas. Current coal gasification consists of partial combustion blowing air or O_2 at temperature well above 1000°C. In addition, gasification-integrated plants require many steps of downstream treatment such as cleaning impurities and adjusting ratio of H_2 and CO (in case of production of liquid fuels and/or chemicals). Accordingly, it results in loss of chemical energy and increase of the associated costs. Advancement of gasification is expected to reduce or even eliminate such problems. Complete coal gasification at low temperature would lead to minimal degrees of chemical energy loss and downstream treatments. However, considerable technical issues should be resolved for realization of the advanced gasification. As reviewed by Hayashi et al. [11], the lowest rank of coal, lignite, is favored feedstock for the low temperature gasification, and its key chemical reactions are associated with catalytic behavior of metallic species and chemical interaction between the solid and gas. Details will be described in this chapter.

1.2. Overview of thermochemical conversion of coal

Coal gasification is a thermochemical or thermo-catalytic process that converts the coal into syngas, by oxidation with O_2, CO_2 and/or H_2O. The process of thermochemical conversion is briefly depicted in **Fig. 1**. The primary conversion step of the gasification is *intra-particle* pyrolysis that produces carbon-enriched solid, termed char, and volatile matter consisting of inorganic gases (H_2, H_2O, CO and CO_2), light hydrocarbons (C_1-C_5) and tar ($\geq C_6$). Char and volatile matter undergo in parallel the exothermic oxidation with O_2 and endothermic oxidation with CO_2 or H_2O. Tar is a complex mixture of aromatic compounds as fragments of coal macromolecules with molecular mass up to 600. It is believed that the tar vapor undergoes further aromatization (removal of aliphatic and oxygen containing substituents), growth in ring size (number of fused/condensed rings) leading to solid (soot), while being converted to the syngas.

The gasification can produce electricity more efficiently than conventional pulverized coal combustion when integrated into the combined power generation cycles with gas/steam turbines. In the integrated coal gasification combined cycles (hereafter referred to as IGCC), the yield of syngas on the basis of coal's chemical energy (i.e., cold gas efficiency) is crucial for the electrical efficiency of power generation, regardless of the system configuration.

Decreasing consumption of O_2 while increasing that of CO_2/H_2O theoretically improves the efficiency, but results in lower temperature for the gasification, potentially causing problems arisen from incomplete conversion of coal. This is a main reason why the gasification of IGCC is operated at temperature well above 1000°C. Decreasing O_2 loading/consumption (lowering temperature) may allow survival of the tar that is a most problematic material at downstream processes such as gas cleaning and combustion. Complete coal conversion and tar removal at temperature below 1000°C are thus important technical issues for utilizing high-efficient gasification.

Consumption of H_2O is kinetically favored rather than that of CO_2 due to its high reactivity on not only char gasification but also reforming of tar vapor. H_2O gasification of char is higher than CO_2 gasification regardless of coal rank [12,13]. Moreover, it is believed that the addition of H_2O produces higher quality syngas [14], promoting water gas shift reaction that generates more H_2 and CO_2 [15]. In addition, prediction of H_2O gasification based on thermodynamic properties also shows performance superior to that of CO_2 one in terms of cold gas efficiency as shown in **Fig. 2**. Despite the advantages, the application of H_2O to a practical gasifier often faces problems in its feeding caused by the latent heat supply throughout the pipelines. Even if the gasification is more efficient, such energy consumption

may reduce overall performance of a plant. Ishii et al. [16] numerically examined the effect of additional supply of H_2O provided from a steam turbine in oxy-fuel IGCC, and concluded that internal supply of H_2O decreases net thermal efficiency. In contrast, CO_2 requires no additional energy consumption and no concerns of condensation. It is inexpensive and abundant, and its utilization is favorable for reducing carbon emissions. Thus, CO_2 has economic, energy-efficient and environmental-friendly advantages compared with H_2O as a gasifying agent. The low reactivity of CO_2 can be compensated by high reactivity of lignite in gasification promoted catalytically, as described later. Further, no or little catalyst from char matrix is lost by volatilization during CO_2 gasification, which is significant in H_2O gasification.

1.3. Catalysis and deactivation of inherent metallic species

Char gasification is known as rate-determining step in the conversion process of coal to syngas, and its reactivity is generally dependent on rank of parent coal. The rate of gasification of char derived from lignite, of which carbon content below 70 wt%, is higher than that from sub-bituminous or higher rank coals [17]. It is mainly arisen from the presence

of alkali and alkaline earth metallic (AAEM) species such as Na and Ca that can be transformed into particles having catalytic activity. There have been numerous studies on the catalytic role of AAEM species [18–24]. Lignite inherently contains abundant AAEM species dispersed highly in its organic matrix in a form of organically bound cation (e.g. $–COO^{-}Na^{+}$) or pore-condensed inorganic salts (e.g. NaCl) [25,26]. The AAEM species are transformed into nano-sized or greater particles in forms of metals, oxides or carbonates during pyrolysis. The catalytic activity of lignite in gasification is expected to completely convert the coal at temperature below 1000°C.

On the other hand, deactivation of catalysis should be simultaneously considered to understand the catalytic behavior. The catalytic particles undergo further growth in size during gasification as its concentration increases, and then self-deactivation takes place because sub-micron sized or greater particles have lower activity than that of the nano-sized one. The AAEM species can be deactivated by reactions with inherent and/or extraneous silica, alumina and aluminosilicates [27–31]. In thermodynamic point of view, such reactions are favored at the temperature range of pyrolysis and gasification. Kannan and Richards [27] confirmed the deactivation by silicate formation by performing CO_2 gasification of biomass mixed with silica, and claimed that the deactivation occurs ‘before gasification’ i.e. ‘during

pyrolysis', because CO_2 suppresses the silicate formation. Similar results were reported in CO_2 gasification of chars derived from lignite [32] and biomass [33], leaving no evidence of deactivation induced by silicate formation.

1.4. Tar decomposition enhanced by interaction with char

Removal of tar is crucial particularly for low temperature gasification due to much of its survival. Although homogeneous reforming of tar is difficult even in the presence of H_2O and/or O_2 [11], interaction with char promotes tar decomposition on its surface. It is believed that tar vapor undergoes decomposition in a sequence of adsorption onto micropores, coke deposition and gasification with oxidants, if any [34]. The coke deposition deactivates the char activity toward tar vapor, and the following gasification regenerates the active micropores.

There have been many studies on decomposition of nascent tar in the presence of char [34–50]. Song et al. [36,50] conducted biomass-derived nascent tar decomposition over nascent char and found that thicker char bed, formed by accumulation of feedstock, reduced tar yield effectively. Abundant radicals from thermal cracking of volatile attack and

decompose tar molecule adsorbed to the char. However, the tar decomposition was not proportional to the bed thickness, because the radicals are too reactive to travel far. Smaller aromatic rings were more refractory than larger ones, particularly that having penta-cycle rings. Matsuhara et al. [35] performed decomposition of nascent tar over lignite char bed and showed a negative coke yield due to fast progress of steam gasification of coke/char at 900 °C. Similar results were reported by Zhang et al. [48] who investigated tar decomposition by co-feeding lignite char, non-activated and steam-activated ones, and its parent coal by changing the blending ratio. The co-feeding of steam-activated char at ratio of 1 decreased tar yield by over 95 %-mol-C. Similar studies were also conducted by applying model tar compounds over char bed [50–56].

Although the degree of decomposition of nascent and model tars is different depending on the experimental conditions, common conclusions of the studies can be drawn: (1) light aromatics are more refractory than heavy ones, (2) char activity significantly increases with activation (or partial gasification), (3) deactivation of char is arisen from coking onto micro- and/or meso-pores, (4) the deactivated pores can be regenerated by gasification, (5) a certain level of char activity remains after deactivation unless *in situ* gasification occurs.

1.5. Scope of the thesis

Lignite gasification with CO_2 is expected to be applicable to a next generation gasification technology. High reactivity of lignite arisen from inherent metallic species as catalysts enables to improve cold gas efficiency by lowering gasification temperature. Kinetic analysis of catalytic and non-catalytic gasification has been conducted in many researches, however none of study has focused on deactivation of catalysts by SiO_2. Lignite contains inherent SiO_2 together with the metallic species, and it is thermodynamically favored to form silicates at gasification conditions. In addition, gasification at temperature below 1000 °C may lead to incomplete decomposition of tar. Successful tar removal is a crucial technical issue for realization of low temperature gasification technology. Lignite char, known to active to tar vapor, is indispensable for the tar removal at lowered temperature, but understanding of its kinetics and mechanism is insufficient.

Purpose of this study is to investigate mechanism of the some key reactions in lignite gasification, i.e. catalysis deactivation induced by SiO_2 and kinetic analysis of tar decomposition over char surface, particularly for temperature below 1000 °C, through kinetic analysis. Further, methods for kinetic measurement are re-evaluated for precise analysis of catalytic and non-catalytic gasification.

The thesis consists of five chapters, and summary of each chapter is as follows:

Chapter 1: General Introduction

The first chapter introduces backgrounds associated with perspective of CO_2 gasification of lignite toward low temperature gasification. Thermochemical conversion of coal is overviewed, and key chemical reactions dealt with in this study are briefly described.

Chapter 2: Kinetics and Mechanism of Deactivation of Inherent Catalyst in CO_2 Gasification of Lignite Char

Highly reactive catalytic gasification is a characteristic of lignite containing abundant metallic species as catalysts. Mechanism of such catalytic promotion has been widely studied, but there has been no research on deactivation of the catalysts. Understanding of mechanism of catalyst deactivation is important for designing a future gasifier. From thermodynamic viewpoint, SiO_2 deactivates inherent catalysts by forming silicates. Extraneous SiO_2 was blended to lignite. Dispersed SiO_2 on carbon matrix was formed by a sequence of briquetting at mechanical pressure of 128 MPa heating up to 200 °C and carbonization at peak temperature of 1000 °C. Coke was gasified with CO_2 at isothermal temperature of 900 °C employing a thermogravimetric analyzer, and kinetic analysis was performed by applying a

parallel reaction model consists of catalytic and non-catalytic terms. Mechanism of catalyst deactivation was then examined.

Chapter 3: Kinetics and Mechanism of Decomposition of Benzene over Lignite Char

Removal of tar is indispensable for development of low temperature gasification. Lignite char is capable to decompose tar vapor through adsorption on its surface. There have been researches on decomposition of aromatic vapor on char bed, however it was suspected that contact time was too long to examine the decomposition mechanism. A new method for continuous measurement was proposed. Residence time on char bed was set to as small as 7.6 ms. Decomposition of benzene, the most refractory compound of tar, was conducted on lignite char bed. Demineralized char and that partially gasified with CO_2 up to conversion of 0.6 were compared. Benzene vapor passed through the bed at temperature of 900 °C carried by N_2 flow. Activity and capacity of each char were investigated. Mechanism of benzene decomposition over char surface was examined.

Chapter 4: Methods for Precise Kinetics Measurement/Analysis of Non-Catalytic and Catalytic CO_2 Gasification of Lignite Char

Kinetics of char gasification is generally performed in a thermogravimetric analyzer. It derives important parameters for designing and operating a gasifier. Fixed bed of char sample placed in a crucible is gasified at designated temperature, flow rate and gas composition. Theoretically, a monolayer is desirable for minimizing heat and mass transport effects. In the sense, sufficiently high flow rate and small particle size are essential to avoid resistances of inter- and intra-particle diffusion. Some researches are however suspected that inaccurate kinetic data have been derived due to such diffusional limits. In addition, differences of mass transport in catalytic and non-catalytic gasification have been hardly paid attention. Lignite char and demineralized one were compared for examining such differences. Effects of total gas flow rate, particle size and sample amount (i.e., bed thickness) were investigated to determine conditions for precise kinetic analysis.

Chapter 5: General Conclusions

Findings and conclusions in each chapter are briefly summarized, and general conclusion is drawn.

References

[1] J.-i. Hayashi, K. Mae, Carbon Neutral/Negative Coproduction of Power and Storable Carbon Resource from Fossils and Biomass, The 82nd SCEJ Annual Meeting, Tokyo, 2016.

[2] G.-j. Liu, Z. Li, M.-h. Wang, W.-d. Ni, Energy savings by co-production: A methanol/electricity case study, Applied Energy 87 (2010) 2854–2859.

[3] H. Lin, H. Jin, L. Gao, W. Han, Economic analysis of coal-based polygeneration system for methanol and power production, Energy 35 (2010) 858–863.

[4] A. Narvaez, D. Chadwick, L. Kershenbaum, Small-medium scale polygeneration systems: Methanol and power production, Applied Energy 113 (2014) 1109–1117.

[5] Y. Qian, J. Liu, Z. Huang, A. Kraslawski, J. Cui, Y. Huang, Conceptual design and system analysis of a poly-generation system for power and olefin production from natural gas, Applied Energy 86 (2009) 2088–2095.

[6] L. Zhou, S. Hu, Y. Li, Q. Zhou, Study on co-feed and co-production system based on coal and natural gas for producing DME and electricity, Chemical Engineering Journal 136 (2008) 31–40.

[7] K.S. Ng, N. Zhang, J. Sadhukhan, Techno-economic analysis of polygeneration systems with carbon capture and storage and CO_2 reuse, Chemical Engineering Journal 219 (2013) 96–108.

[8] Z. Li, P. Liu, F. He, M. Wang, E.N. Pistikopoulos, Simulation and exergoeconomic analysis of a dual-gas sourced polygeneration process with integrated

methanol/DME/DMC catalytic synthesis, Computers and Chemical Engineering 35 (2011) 1857–1862.

[9] Y.K. Salkuyeh, T.A. Adams II, Co-Production of Olefins, Fuels, and Electricity from Conventional Pipeline Gas and Shale Gas with Near-Zero CO_2 Emissions. Part I: Process Development and Technical Performance, Energies 8 (2015) 3739-3761.

[10] Y.K. Salkuyeh, T.A. Adams II, Co-Production of Olefins, Fuels, and Electricity from Conventional Pipeline Gas and Shale Gas with Near-Zero CO2 Emissions. Part II: Economic Performance**,** Energies 8 (2015) 3762-3774.

[11] J.-i. Hayashi, S. Kudo, H.-S. Kim, K. Norinaga, K. Matsuoka, S. Hosokai, Low-Temperature Gasification of Biomass and Lignite: Consideration of Key Thermochemical Phenomena, Rearrangement of Reactions, and Reactor Configuration, Energy Fuel 28 (2014) 4–21.

[12] D.P. Ye, J.B. Agnew, D.K. Zhang, Gasification of a South Australian low-rank coal with carbon dioxide and steam: kinetics and reactivity studies, Fuel 77 (1998) 1209–1219.

[13] L. Zhang, J. Huang, Y. Fang, Y. Wang, Gasification Reactivity and Kinetics of Typical Chinese Anthracite Chars with Steam and CO_2, Energy Fuels 20 (2006) 1201–1210.

[14] J. Gil, J. Corella, M.P. Aznar, M.A. Caballero, Biomass gasification in atmospheric and bubbling fluidized bed: Effect of the type of gasifying agent on the product distribution, Biomass Bioenergy 17 (1999) 389–403.

[15] C. Fushimi, K. Araki, Y. Yamaguchi, A. Tsutsumi, Effect of Heating Rate on Steam Gasification of Biomass. 2. Thermogravimetric-Mass Spectrometric (TG-MS) Analysis of Gas Evolution, Ind. Eng. Chem. Res. 42 (2003) 3929–3936.

[16] H. Ishii, T. Hayashi, H. Tada, K. Yokohama, R. Takashima, J.-i. Hayashi, Critical assessment of oxy-fuel integrated coal gasification combined cycles, Applied Energy 233–234 (2019) 156–169.

[17] K. Miura, K. Hashimoto, P.L. Silveston, Factors affecting the reactivity of coal chars during gasification, and indices representing reactivity, Fuel 68 (1989) 1461–1475.

[18] E.J. Hippo, R.G. Jenkins, P.L. Walker Jr., Enhancement of lignite char reactivity to steam by cation addition, Fuel 58 (1979) 338–344.

[19] T.D. Hengel, P.L. Walker Jr., Catalysis of lignite char gasification by exchangeable calcium and magnesium, Fuel 63 (1984) 1214–1220.

[20] Y. Ohtsuka, A. Tomita, Calcium catalysed steam gasification of Yallourn brown coal, Fuel 65 (1986) 1653–1657.

[21] C.S.-M. de Lecea, M. Almela-Alarcoń, A. Linares-Solano, Calcium-catalysed carbon gasification in CO_2 and steam, Fuel 69 (1990) 21–27.

[22] A. Linares-Solano, C.S.-M. de Lecea, D. Cazorla-Amoros, J.P. Joly, H. Charcosset, Nature and Structure of Calcium Dispersed on Carbon, Energy Fuels 4 (1990) 467–474.

[23] Y. Ohtsuka, K. Asami, Ion-Exchanged Calcium from Calcium Carbonate and Low-Rank Coals: High Catalytic Activity in Steam Gasification, Energy Fuels 10 (1996) 431–435.

[24] D.M. Quyn, H. Wu, J.-i. Hayashi, C.-Z. Li, Volatilisation and catalytic effects of alkali and alkaline earth metallic species during the pyrolysis and gasification of Victorian brown coal. Part IV. Catalytic effects of NaCl and ion-exchangeable Na in coal on char reactivity, Fuel 82 (2003) 587–593.

[25] J-i. Hayashi, K. Miura, Chapter 4 - Pyrolysis of Victorian brown coal, in: C.-Z. Li (Eds.), Advances in the Science of Victorian Brown Coal, Elsevier, Amsterdam, 2004, pp. 134–222. doi:10.1016/B978-008044269-3/50005-4.

[26] A. Tomita, Y. Ohtsuka, Chapter 5 - Gasification and Combustion of Brown Coal, in: C.-Z. Li (Eds.), Advances in the Science of Victorian Brown Coal, Elsevier, Amsterdam, 2004, pp. 223–285. doi:10.1016/B978-008044269-3/50006-6.

[27] M.P. Kannan, G.N. Richards, Gasification of biomass chars in carbon dioxide: dependence of gasification rate on the indigenous metal content, Fuel 69 (1990) 747–753.

[28] H. Risnes, J. Fjellerup, U. Henriksen, A. Moilanen, P. Norby, K. Papadakis, D. Posselt, L.H. Sørensen, Calcium addition in straw gasification, Fuel 82 (2003) 641–651.

[29] G. Bruno, M. Buroni, L. Carvani, G. Del Piero, G. Passoni, Water-insoluble compounds formed by reaction between potassium and mineral matter in catalytic coal gasification, Fuel 67 (1988) 67−72.

[30] L. Kühn, H. Plogmann, Reaction of catalysts with mineral matter during coal gasification, Fuel 62 (1983) 205−208.

[31] T. Okuno, N. Sonoyama, J.-i. Hayashi, C.-Z. Li, C. Sathe, T. Chiba, Primary Release of Alkali and Alkaline Earth Metallic Species during the Pyrolysis of Pulverized Biomass, Energy Fuels 19 (2005) 2164−2171.

[32] E. Byambajav, Y. Hachiyama, S. Kudo, Koyo Norinaga, J.-i. Hayashi, Kinetics and Mechanism of CO_2 Gasification of Chars from 11 Mongolian Lignites, Energy Fuels 2016, 30, 1636−1646.

[33] Z.F. Zahara, S. Kudo, Daniyanto, U.P.M. Ashik, K. Norinaga, A. Budiman, J.-i. Hayashi, CO_2 Gasification of Sugar Cane Bagasse: Quantitative Understanding of Kinetics and Catalytic Roles of Inherent Metallic Species, Energy Fuel 32 (2018) 4255–4268.

[34] S. Hosokai, K. Kumabe, M. Ohshita, K. Norinaga, C.-Z. Li, J.-i. Hayashi, Mechanism of decomposition of aromatics over charcoal and necessary condition for maintaining its activity, Fuel 87 (2008) 2914–2922.

[35] T. Matsuhara, S. Hosokai, K. Norinaga, K. Matsuoka, C.-Z. Li, Jun-ichiro Hayashi, In-Situ Reforming of Tar from the Rapid Pyrolysis of a Brown Coal over Char, Energy Fuels 24 (2010) 76–83.

[36] Y. Song, , Y, Wang, X. Hu, J. Xiang, S. Hu, D. Mourant, T. Li, L. Wu, C.-Z. Li, Effects of volatile–char interactions on *in-situ* destruction of nascent tar during the pyrolysis and gasification of biomass. Part II. Roles of steam, Fuel 143 (2015) 555–562.

[37] M.L. Boroson, J.B. Howard, J.P. Longwell, W.A. Peters, Heterogeneous Cracking of Wood Pyrolysis Tars over Fresh Wood Char Surfaces, Energy Fuels 1989, 3, 735–740.

[38] P. Brandt, E. Larsen, U. Henriksen, High Tar Reduction in a Two-Stage Gasifier, Energy Fuels 2000, 14, 816–819.

[39] O. Mašek, N. Sonoyama, E. Ohtsubo, S. Hosokai, C.-Z. Li, T. Chiba, J.-i. Hayashi, Examination of catalytic roles of inherent metallic species in steam reforming of nascent volatiles from the rapid pyrolysis of a brown coal, Fuel Process. Technol. 2007, 88, 179–185.

[40] Z. Abu El-Rub, E.A. Bramer, G. Brem, Experimental comparison of biomass chars with other catalysts for tar reduction, Fuel 87 (2008) 2243–2252.

[41] A. Dufour, A. Celzard, V. Fierro, E. Martin, F. Broust, A.Zoulalian, Applied Catalysis A: General 346 (2008) 164–173.

[42] P. Gilbert, C. Ryu, V. Sharifi, J. Swithenbank, Tar reduction in pyrolysis vapours from biomass over a hot char bed, Bioresource Technology 100 (2009) 6045–6051.

[43] S. Hosokai, K. Norinaga, T. Kimura, M. Nakano, C.-Z. Li, J.-i. Hayashi, Reforming of Volatiles from the Biomass Pyrolysis over Charcoal in a Sequence of Coke Deposition and Steam Gasification of Coke, Energy Fuels 25 (2011) 5387–5393.

[44] D. Wang, W. Yuan, W. Ji, Char and char-supported nickel catalysts for secondary syngas cleanup and conditioning, Applied Energy 88 (2011) 1656–1663.

[45] J.-i. Hayashi, H. Takahashi, M. Iwatsuki, K. Essaki, A. Tsutsumi, T. Chiba, Rapid conversion of tar and char from pyrolysis of a brown coal by reactions with steam in a drop-tube reactor, Fuel 79 (2000) 439–447.

[46] J.-I. Hayashi, M. Iwatsuki, K. Morishita, A. Tsutsumi, C.-Z. Li, T. Chiba, Roles of inherent metallic species in secondary reactions of tar and char during rapid pyrolysis of brown coals in a drop-tube reactor, Fuel 81 (2002) 1977–1987.

[47] Z. Min, P. Yimsiri, M. Asadullah, S. Zhang, C.-Z. Li, Catalytic reforming of tar during gasification. Part II. Char as a catalyst or as a catalyst support for tar reforming, Fuel 90 (2011) 2545–2552.

[48] L.-x. Zhang, T. Matsuhara, S. Kudo, J.-i. Hayashi, K. Norinaga, Rapid pyrolysis of brown coal in a drop-tube reactor with co-feeding of char as a promoter of in situ tar reforming, Fuel 112 (2013) 681–686.

[49] L.-x. Zhang, S. Kudo, N. Tsubouchi, J.-i. Hayashi, Y. Ohtsuka, K. Norinaga, Catalytic effects of Na and Ca from inexpensive materials on in-situ steam gasification of char from rapid pyrolysis of low rank coal in a drop-tube reactor, Fuel Processing Technology 113 (2013) 1–7.

[50] Y. Song, Y. Wang, X. Hu, S. Hu, J. Xiang, L. Zhang, S. Zhang, Z. Min, C.-Z. Li, Effects of volatile–char interactions on in situ destruction of nascent tar during the pyrolysis and gasification of biomass. Part I. Roles of nascent char, Fuel 122 (2014) 60–66.

[51] M. Morgalla, L. Lin, M. Strand, Decomposition of benzene using char aerosol particles dispersed in a high-temperature filter, Energy 118 (2017) 1345–1352.

[52] M. Morgalla, L. Lin, M. Strand, Benzene conversion in a packed bed loaded with biomass char particles, Energy Fuels 32 (2018) 554–560.

[53] L. Burhenne, T. Aicher, Benzene removal over a fixed bed of wood char: The effect of pyrolysis temperature and activation with CO_2 on the char reactivity, Fuel Process. Tech. 127 (2014) 140–148.

[54] F. Nestler, L. Burhenne, M.J. Amtenbrink, T. Aicher, Catalytic decomposition of biomass tars: The impact of wood char surface characteristics on the catalytic performance for naphthalene removal, Fuel Process. Tech. 145 (2016) 31–41.

[55] D. Fuentes-Cano, A. Gómez-Barea, S. Nilsson, P. Ollero, Decomposition kinetics of model tar compounds over chars with different internal structure to model hot tar removal in biomass gasification, Chem. Eng. J. 228 (2013) 1223–1233.

[56] D. Fuentes-Cano, F. Parrillo, G. Ruoppolo, A. Gómez-Barea, U. Arena, The influence of the char internal structure and composition on heterogeneous conversion of naphthalene, Fuel Process. Tech. 172 (2018) 125–132.

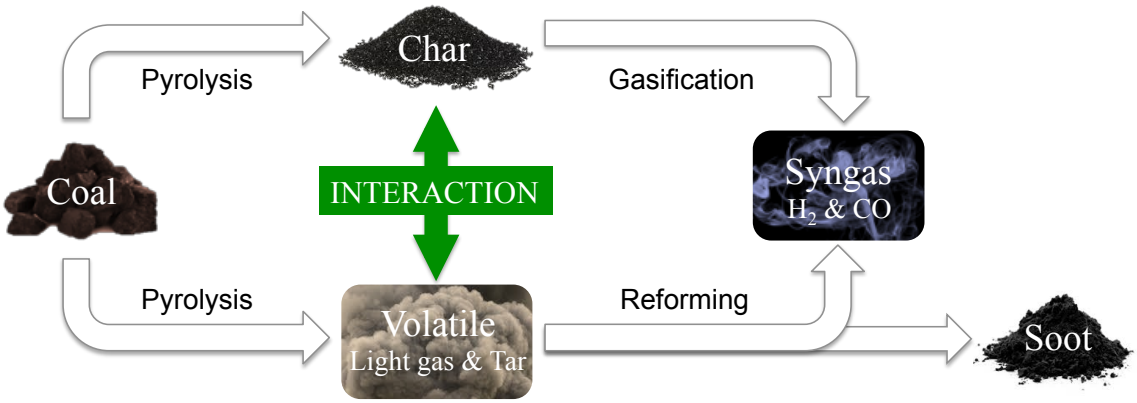

Fig. 1 Process of thermochemical conversion of coal to syngas

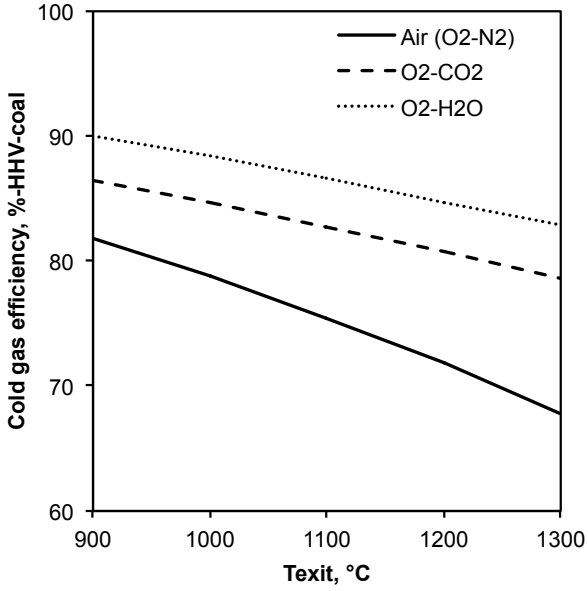

Fig. 2 Thermodynamic prediction of changes in cold gas efficiency depending on the gasifying agent, calculated from following assumptions; (a) Gasifier consists of two reactors: combustor and reductor. (b) Elemental composition of coal is $CH_{0.74}O_{0.08}$, and it contains 5 wt% of moisture. (c) The coal and gasifying agents are fed into the gasifier at temperatures of 25 and 200°C, respectively. (d) Products consist solely of H_2, H_2O, CO, and CO_2. (e) Product gases at the exit of combustor and reductor are in the state of chemical equilibrium. (f) Residual char from the reductor is recycled to the combustor, and is completely burned. (g) Elemental composition of the char is $CH_{0.174}$, and its specific heat is 0.012 kJ/mol-K. (h) Heat loss of the gasifier is 3 % of coal's LHV.

Chapter 2

Kinetics and Mechanism of Deactivation of Inherent Catalyst in CO_2 Gasification of Lignite Char

2.1. Introduction

Reaction of carbonized coal, which is termed coke or char, with carbon dioxide (CO_2) has technical and scientific significance because of its application to production of iron in blast furnace and that of syngas (H_2 and CO) in gasifier. The coke/char reaction with CO_2 is hereafter termed CO_2 gasification, or just gasification. It is known that coke/char derived from low-rank coal of lignite to sub-bituminous ranks has much higher reactivity with CO_2 than that from coal of bituminous or higher rank. Such high reactivity arises mainly from catalysis of inherent metallic species such as Na, Ca and Fe that are highly dispersed in the organic matrix of coal in forms of organically bound cations or pore-condensed inorganic salts [1-4]. In the course of pyrolysis, such metallic species transform into nano-sized or greater particles (metals, oxides or carbonates) that can catalyze the gasification forming redox cycles. The activity of such nano-sized particles is much higher than that of bulk mineral particles with sub-micron and greater sizes.

Use of low-rank coal in the gasification to produce syngas is attractive because the catalytic promotion of the gasification of char (as an intermediate) is favored for increasing the overall coal conversion into syngas and cold gas efficiency (by lowering the operating temperature). The low-rank coal is potentially applicable to ironmaking. The present authors [5-7] developed a sequence of binderless hot briquetting at temperatures up to 200°C and carbonization at 900–1000°C to convert lignite into coke with tensile strength as high as 10–40 MPa. Suppose that low-rank-coal derived coke is fed into the blast furnace, it is expected that the catalytic promotion of coke gasification enhances the iron productivity by decreasing

the gas/solid temperature in the thermal reserve zone of the blast furnace [8], while significantly changing operating variables. Use of "*highly or excessively reactive coke*" is not necessarily accepted from a viewpoint of stable operation of the furnace. Thus, technical options of not only taking advantage of "*high reactivity*" but also "*controlling the reactivity*" are possible in the future use of low-rank-coal derived coke.

Chemical and physical behaviors of catalysts in the coke/char gasification are complex. As progress of the gasification, in other words, that of carbon loss increases the catalyst concentration. This induces the catalytic particles to grow in size and thereby deactivating them. Another type of deactivation is caused by reactions of catalytic species with silica (SiO_2), alumina (Al_2O_3) and aluminosilicates [9,10]. Reactions of Na and Ca with SiO_2 and Al_2O_3 are both favored thermodynamically over the temperature range relevant to the carbonization as well as gasification [11]. The catalyst deactivation (pertains to the catalyst precursor) can occur even prior to the gasification [7].

Some recent studies made focal points on the deactivation of inherent catalysts during and prior to CO_2 gasification [12-15]. Byambajav et al. [12] studied CO_2 gasification of chars from various types of Mongolian lignites. They performed kinetic analysis by employing a comprehensive model that assumed progress in parallel of non-catalytic gasification and inherent-metallic-species-catalyzed gasification [13,14]. The model enabled to describe the rate of gasification quantitatively over the entire range of char conversion (0 to 0.999 or even higher). They demonstrated that the effective amount of catalyst (based on the rate of catalytic gasification) at the beginning of gasification was correlated well with either (Na+Ca)/Si or (Na+Ca+Fe)/Si molar ratio for 11 types of chars from the different lignites. Conversely, the rate of catalyst deactivation during the gasification did not correlate with either ratio mentioned above or with the Si content of the char. Zahara et al. [15] investigated CO_2 gasification of chars from 12 different types of sugarcane bagasses, and reported results of kinetic analysis, which were qualitatively very similar to those by Byambajav et al. [12]. Zahara et al. [15] also claimed that the inherent catalyst underwent deactivation by reacting with SiO_2 prior to the gasification, i.e., during the pyrolysis, while suspected the occurrence of SiO_2-induced deactivation during the gasification.

Herein, the present authors investigate the mechanism of CO_2 gasification of coke from a type of lignite with a very low ash content. This places a strong focus on the deactivation of the inherent catalyst due to its reaction with SiO_2 before the gasification and that during the gasification. This paper proposes a new method to examine the role of SiO_2 in the catalyst deactivation through a newly designed coke preparation and kinetic-analysis/modeling of the coke gasification.

2.2. Experimental

2.2.1. Materials

A type of Victorian lignite, Loy Yang, was dried at 40°C under reduced pressure until its moisture content decreased to 8–10 wt% on a wet basis, and then pulverized to sizes smaller than 106 μm. The elemental composition of the lignite was as follows: C; 66.9, H; 4.8, N; 0.6, O+S; 27 wt% (by difference) on a dry-ash-free basis. The ash content was 0.8 wt% on a dry basis. Commercially available high-purity SiO_2 (CAS: 7631-86-9, Aldrich) was used without any pretreatment. Preliminary observation of the SiO_2 by scanning electron microscopy (SEM) confirmed that it consisted of particles with sizes of around 100 nm. The pulverized lignite and SiO_2 were mixed at a prescribed mass ratio, and subjected to ball milling for 10 h at ambient temperature. Balls made of ZrO_2 with diameters of 10 mm were employed for the milling. SiO_2-blended lignite samples with different SiO_2 mass fractions were thus prepared. The pulverized lignite was also ball-milled under the same conditions as mentioned above but without SiO_2. The SEM observation of the lignite particles after the ball milling showed that it reduced the particle sizes to less than 10 μm.

The lignite was also washed sequentially with aqueous solutions of hydrochloric acid (HCl, concentration; 3.0 mol/L) and hydrofluoric acid (HF, 3.0 mol/L) at 60°C referring to the procedures reported by Sugano et al. [16] and Liu et al. [17] The purpose of the acid treatment was to remove the inherent metallic species as much as possible and to know the kinetics of non-catalytic gasification of coke. Another acid treatment with only the aqueous

solution of HCl (3.0 mol/L) was also applied for examining the effectiveness of using HF on the removal of metallic species.

2.2.2. Experimental and analytical methods

The ball-milled lignite and lignite/SiO_2 blends were briquetted by applying temperature and mechanical pressure of 200 °C and 128 MPa, respectively. Every briquette was in form of disc with diameter and thickness of 14 mm and 5 mm, respectively. Details of the procedure were reported elsewhere [5,6]. The briquettes with different contents of SiO_2, f_{SiO2} = 0, 4.6, 9.2 and 13.7 wt%-briquette, were thus prepared. The briquettes were converted to cokes by heating under atmospheric flow of nitrogen (N_2, purity > 99.9999 vol%). The heating rate, peak temperature and holding time were 5 °C min^{-1}, 1000°C, and 10 min, respectively. The bulk density and tensile strength of every coke sample were measured in the same ways as reported previously [5,6].

Every coke sample was crushed and pulverized to sizes smaller than 106 μm, and then subjected to CO_2 gasification in a thermogravimetric analyzer (TGA; Hitachi Hi-Tech Science Corporation, model STA7200). This TGA had a high thermogravimetric sensitivity of 0.2 μg. A portion (*ca*. 2 mg) of the sample was placed in a platinum-made pan, set properly in the TGA, and heated in atmospheric N_2 flowing at 700 ml-stp/min up to the holding temperature of 900±2°C. After confirming stabilization of the sample mass as well as temperature, the flowing gas was switched to an atmospheric CO_2/N_2 mixture (50/50 in vol.) at the same flow rate as above for starting the gasification. The procedure of the gasification was originally designed in order to eliminate the effects of extra- and intra-particle mass transport processes on the kinetics of gasification as reported previously [12,15].

The contents of metallic species in the lignite were quantified according to a reported procedure [7]. The contents of Na, K, Mg, Ca and Fe were 0.079, 0.012, 0.062, 0.058 and 0.067 wt%-dry, respectively. The total contents of the oxides from these metallic species, i.e., Na_2O, K_2O, MgO CaO and Fe_2O_3 were then 0.40 wt%-dry. Neither of the SiO_2 nor Al_2O_3 content was measured, but was estimated as low as *ca.* 0.4 wt%-dry in total from the

difference between the total ash content and that contributed by the Na, K, Mg, Ca and Fe oxides.

2.2.3. Kinetic modeling

The overall rate of char gasification is described by the sum of the rates of non-catalytic gasification and catalytic gasification (Eqn. 1) [13,14,18]

$$\frac{dX}{dt} = k_{\mathrm{nc}}(1 - X) + \sum_n k_{\mathrm{C}n} \quad (1)$$

k_{nc} and $k_{\mathrm{C}n}$ are the first-order rate constant for the non-catalytic gasification and the zero-th-order one for the catalytic gasification, respectively [12,15]. n indicates the catalytic component Cn (n = 1, 2, 3, ⋯). $k_{\mathrm{C}n}$ is given as the product of the effective amount of catalyst ($m_{\mathrm{C}n}$) and rate constant (k'_{C}).

$$k_{\mathrm{C}n} = k'_{\mathrm{C}} m_{\mathrm{C}n} \quad (2)$$

$$k_{\mathrm{C}n,0} = k'_{\mathrm{C}} m_{\mathrm{C}n,0} \text{ (at } t = 0) \quad (3)$$

Eqns. 2 and 3 assume that the rate of catalytic gasification is determined not by the concentration but by the amount of catalyst dispersed in the coke matrix [13-15,20]. This is because such catalyst is always surrounded by the carbonaceous matter unless the char conversion is extremely high. $k_{\mathrm{C}n}$ is defined as the activity of Cn catalysts, while k'_{C} is common among the catalysts with different n. On the other hand, the rate of catalyst deactivation should be a function of its concentration regardless of the order of reaction. The catalyst concentration increases along the coke conversion (Eqn. 4).

$$C_{\mathrm{C}n} = \frac{m_{\mathrm{C}n}}{1 - X} \quad (4)$$

The present model assumes first-order kinetics for the deactivation of every catalyst (Eqn. 5). This assumption was originally for expedience, but it was successfully applied to the description of the kinetics of gasification of chars from lignite and biomass in previous studies [12,15].

$$\frac{dm_{Cn}}{dt} = -k_{\text{loss-}n} C_{Cn} = -k_{\text{loss-}n} \frac{m_{Cn}}{1-X} \tag{5}$$

The model also assumes the presence of a catalyst precursor (C1prec) that is transformed exclusively to C1 catalyst obeying first-order kinetics, following success of previous works [12,15]. Its concentration is expressed by

$$\frac{dm_{\text{C1prec}}}{dt} = -k_{\text{C1prec}} C_{\text{C1prec}} = -k_{\text{C1prec}} \frac{m_{\text{C1prec}}}{1-X} \tag{6}$$

Then, the time-dependent changes in the concentration of the catalysts are expressed as follows.

$$\frac{dm_{\text{C1}}}{dt} = k_{\text{C1prec}} C_{\text{C1prec}} - k_{\text{loss-1}} C_{\text{C1}} \tag{7}$$

$$\frac{dm_{Cn}}{dt} = -k_{\text{loss-}n} C_{Cn} \ (n \geq 2) \tag{8}$$

The effective amount of the catalyst at $t = 0$ is defined as

$$\sum_n m_{Cn,0} + m_{\text{C1prec},0} = 1 \tag{9}$$

The overall catalytic activity at $t = 0$, which is referred to as ICA-1 (initial catalytic activity) is a useful parameter. It is presented by

$$\text{ICA-1} = \sum_n k_{Cn,0} = k'_C \sum_n m_{Cn,0} \quad (10)$$

It is also useful to define a potential catalytic activity corresponding to $\sum_n m_{Cn,0} + m_{C1prec,0}$, which is given as ICA-2.

$$\text{ICA-2} = k'_C\left(m_{C1prec,0} + \sum_n m_{Cn,0}\right) = k'_C \quad (11)$$

In addition to ICA-1 and ICA-2, a type of the average rate of catalyst deactivation at $t = 0$ ($k_{\text{loss-ave}}$) is introduced based on the catalyst concentration.

$$k_{\text{loss-ave}} = \frac{\sum_n k_{\text{loss-}n} C_{Cn}}{\sum_n C_{Cn}} \quad (12)$$

$$k_{\text{loss-ave},0} = \frac{\sum_n k_{\text{loss-}n} C_{Cn,0}}{\sum_n C_{Cn.0}} \, (t = 0) \quad (13)$$

2.3. Results and Discussion

2.3.1. Dispersion of SiO_2 particles in the briquette/coke matrices

It was necessary to confirm intimate contact between SiO_2 particles in the coke matrix for employing the SiO_2/lignite blend as coal that contains both highly dispersed metallic species and SiO_2 particles in its organic matrix. This section reports physical properties of the cokes and briquettes, and discusses the extent and mode of the particle dispersion in the carbonaceous matrix. For in depth kinetic examination, a 'simulation' of coal that contains

SiO_2 as a mineral and dispersed metallic species as catalysts is successfully demonstrated. Results of kinetic analysis of gasification are reported in the section 3.2.

Fig. 1 shows the effect of f_{SiO2} on the coke yield. The straight line drawn in the graph indicates the coke yield that is calculated by assuming no physical/chemical effect of SiO_2 on the pyrolysis/carbonization of the briquette, and no mass release from the SiO_2 as well. The good agreement between the measured and calculated yields shows that the SiO_2 behaved as a non-catalytic material.

Fig. 2 presents the tensile strength of coke as a function of f_{SiO2}. The SiO_2 contents in the cokes from the blends with f_{SiO2} = 4.6, 9.2 and 13.7 wt%-briquette were 8.2, 15.7 and 22.8 wt%-coke, respectively. The strength of the coke is as high as 25 MPa at f_{SiO2} = 4.6, and in broad agreement with previous reports by the present authors [6,7]. The SiO_2 blending hardly influences the strength up to f_{SiO2} = 9.2 wt% while causes a decrease at greater f_{SiO2}. This trend suggests that the carbonaceous matrix of the coke had strong contact with or even adhesion to SiO_2 particles, which were highly dispersed in the matrix unless the SiO_2 content in the coke was as high as 23 wt%-coke.

Fig. 3 shows the effects of f_{SiO2} on the briquette/coke bulk densities. The true density of SiO_2 is 2.65 g/cm^3, and it is greater than that of the bulk density of the briquette without SiO_2. A slight decrease in the bulk density of the SiO_2-blended briquette with f_{SiO2} suggests that the SiO_2 particles were dispersed in the organic matrix forming porous agglomerates and/or interstices between them and the carbonaceous matrix. The SiO_2 blending thus increased the porosity of briquette. On the other hand, the bulk density of coke increases with f_{SiO2}. Taken together with the trend of the briquette bulk density, this indicates that pores at the SiO_2/matrix interfaces were diminished or shrank during the pyrolysis and carbonization.

The specific volumes of briquette and coke were analyzed. The result for the briquettes is exhibited in **Fig. 4(a)**. The specific volume was calculated by assuming no interstice among SiO_2 particles and also between them and the organic matrix (*see the dashed line in the figure*). From the difference between the measured and calculated volumes, the interstitial volume seems to increase in a manner roughly linear with f_{SiO2}. **Fig. 4(b)** shows the measured and calculated specific volumes of coke in the same manner as for the

briquette. The difference between the measured and calculated volumes becomes significant at $f_{SiO2} > 4.6$ wt%.

The result shown in **Fig. 4(b)** was further analyzed to see the trend shown in **Fig. 5(a)**. The SiO_2-induced pore volume increases in a highly linear manner with the total volume of SiO_2. The intercept suggests that SiO_2 particles were dispersed without forming agglomerates at $f_{SiO2} < 1.8$ wt%-briquette. The slope of the line, 1.05 cm^3-pore/cm^3-SiO_2 enables to estimate the average void fraction of SiO_2 agglomerates (including the interstitial volume between agglomerates and coke matrix) as 0.51, and also that such a void fraction was steady over the range of f_{SiO2} of 4.6–13.7 wt%-briquette. It is reasonable to classify SiO_2 particles into those dispersed as single particles and agglomerates. **Fig. 5(b)** plots the content of agglomerated SiO_2 against total content of SiO_2. It is estimated that the agglomerated SiO_2 occurred at $f_{SiO2} \approx 3.5$ wt%-briquette, over which increase in f_{SiO2} increased the agglomerated SiO_2 exclusively, increasing its fraction.

Fig. 7 exhibits SEM photographs of fractured surfaces of the coke from the SiO_2/lignite blend with $f_{SiO2} = 9.2$ wt%. The size of SiO_2 agglomerates was difficult to measure, but was estimated to be at most several microns. **Fig. 7** compares fractured coke surfaces between $f_{SiO2} = 0$ and 4.6 wt%. It was difficult to detect SiO_2 agglomerates on the fractured coke surfaces for $f_{SiO2} = 4.6$ wt%. This was consistent with the observation that a substantial portion of SiO_2 was dispersed as single particles in the coke matrix.

2.3.2. Kinetic analysis of coke gasification

2.3.2.1. Kinetics of gasification of coke from acid-treated lignite (determination of k_{nc})

Fig. 8 shows characteristics of gasification of cokes from the acid-treated lignites. The gasification of the coke from the HCl/HF-treated lignite occurred very slowly, and it took more than 1,600 min to gasify 99% of the coke. In addition to this, the specific rate ($r_{sp} = dX/dt/(1–X)$) seems to be roughly steady over a range of X up to 0.8, and increases at greater X. The coke from the HCl-treated lignite underwent more rapid gasification than that from the HCl/HF-treated lignite. It was thus concluded that the HCl/HF treatment was necessary to

remove the inherent catalytic metallic species extensively. The removal by the HCl/HF treatment was, however, not necessarily complete, as discussed below.

It is strongly suggested from recent studies on steam gasification or CO_2 gasification [12,15,18] that non-catalytic gasification of chars from lignite and biomass "in the absence of metallic species" obeys first-order kinetics (i.e., steady r_{sp}). Such first-order kinetics is not followed by the gasification of the coke from the HCl/HF-treated lignite at $X > 0.8$. This would arise from a small amount of inherent metallic species left in the HCl/HF-treated lignite. The metallic species, if its concentration is very low, might be dispersed in the carbonaceous matrix, and unable to form "clusters" that have catalysis. The progress of the gasification simply causes an increase in the concentration of the metallic species and probably their supersaturation, inducing their clustering (precipitation of catalytic particles) at a certain conversion of char. The occurrence of the catalysis in such a way is found in earlier reports [19,20]. Based on the above discussion, it is reasonable to define the rate constant for the non-catalytic gasification as $k_{nc} = 0.0021$ min^{-1}, as indicated in **Fig. 8(b)**. r_{sp} for the coke from the HCl-treated lignite increases earlier than that from the HCl/HF-treated lignite. This is reasonably accepted if the coke from the HCl-treated lignite retained greater quantities of metallic species than the HCl/HF treated one.

2.3.2.2. Effect of SiO_2 on the rate of gasification

Fig. 9 presents the conversion profiles for the cokes with different f_{SiO2} over a range of $X = 0$–0.999 on the logarithmic scale. The coke without SiO_2 blend is gasified so quickly that X reaches 0.99 within 80 min, which is as short as 1/20 of that for the coke from the HCl/HF-treated lignite. This demonstrates that the major part of coke was gasified under catalysis of the inherent metallic species. The SiO_2 blend slows down the gasification. The SiO_2 blends with 4.6 and 13.7 wt% extend the time required for 99% coke gasification by factors of 3.6 and 4.8, respectively. It is also seen that such an effect of blending SiO_2 approaches 'saturation' at f_{SiO2} around 10 wt%. The contribution of SiO_2 to the deactivation of catalyst and/or its precursor is thus evidenced.

2.3.2.3. Quantitative model description of the kinetics of coke gasification

Fig. 10 presents measured characteristics of coke gasification for the individual f_{SiO2} and compares them with those predicted by the kinetic model with optimized parameters for the catalytic gasification. The procedure for the parameter optimization was reported previously and in detail by the present authors [12,15]. The model reproduces the kinetics of gasification quantitatively over the entire range of conversion. For the coke without SiO_2 blend, the major part of *dX/dt* arises from the catalytic gasification. It is also noted that *dX/dt* increases gradually up to X = 0.6–0.7, and then decreases quickly. This is explained by the transformation of C1prec into C1 at a rate greater than that of the C1 deactivation as well as that of the other catalysts at X up to 0.6–0.7.

The *dX/dt* for f_{SiO2} = 4.6 and that for 9.2 wt% appear to decrease with X monotonously, but the quantitative description of the *dX/dt*'s requires the assumption of the presence of C1prec. The *dX/dt* for f_{SiO2} = 13.7 wt% is not the case, and it is reproduced well without assuming C1prec. **Table 1** lists the optimized kinetic parameters. It is necessary to assume four catalytic components (C1–C4) in order to reproduce the *dX/dt vs X* and 1–X vs t profiles over the range of X = 0–0.999. It is believed that the catalytic activity and deactivation rate constant distribute over some orders of magnitude. The present kinetic model represents such broad distributions in discrete manners by considering a limited number of catalytic components [12].

Fig. 11 illustrates the effect of f_{SiO2} on the initial catalytic activity. ICA-1 and ICA-2 represent the initial overall catalytic activity and that including the potential activity of C1prec, respectively. Both ICA-1 and ICA-2 decrease with increasing f_{SiO2}, which demonstrates the deactivation of substantial portions of C1 and C1prec before the coke gasification, in other words, during the pyrolysis/carbonization of briquette. The difference between (ICA-2) and (ICA-1), i.e., $k'_C \cdot m_{C1prec,0}$ decreases to zero. It is believed that C1prec consisted of metallic species that were dispersed in the carbonaceous matrix at an atomic or a similar scale, but not yet transformed into nano-sized particles (i.e., C1) at the beginning of gasification. It is also reasonable that such species were mobile enough to easily access SiO_2 particles and react with them during the pyrolysis. It is well known that reactions of Na and

Ca oxides with SiO_2 are thermodynamically favored to form various silicates such as Na_2SiO_3 and $CaSiO_3$ over the temperature range of interest.

The loss of ICA-1 is less extensive than that in (ICA-2) – (ICA-1), and also limited. The major part of the loss of ICA-1 is due to that in $k_{C1,0}$. The C1 was thus more reactive than the other catalytic components (C2–C4). The C1 consisting of nano-sized 'active' particles that had less mobility than C1prec, and its reaction with SiO_2 was slower or less extensive during the pyrolysis/carbonization, or otherwise, the SiO_2 blending caused the formation of less amount of C1 during the pyrolysis/carbonization by converting C1prec into silicates. $k_{C2,0}$ and $k_{C3,0}$ decrease with f_{SiO2} but only slightly. It was believed that C2 and C3 were even less mobile than C1 as well as C1prec. Thus, the kinetic analysis revealed that the SiO_2 deactivated C1 and C1prec substantially and completely, respectively, before the gasification.

$k_{loss\text{-}ave}$, which is defined as $\Sigma k_{loss\text{-}n}C_{Cn}/\Sigma C_{Cn}$, is convenient for discussing overall kinetics of catalyst deactivation. **Fig. 12** shows the trends of change in $k_{loss\text{-}ave}$ for the cokes with different f_{SiO2}. It is clearly seen that $k_{loss\text{-}ave}$ for $f_{SiO2} = 0$ is greater than the others. In other words, the overall rate constant for the catalyst deactivation is even decreased by the presence of SiO_2. There is no indication of SiO_2-induced catalyst deactivation.

The initial $k_{loss\text{-}ave}$'s at $X = 0$ (i.e., $k_{loss\text{-}ave,0}$'s) are plotted against f_{SiO2} in **Fig. 13(a)**. $k_{loss\text{-}ave,0}$ for $f_{SiO2} = 0$ is 0.0052 min^{-1}, and it decreases with increasing f_{SiO2} while approaching *ca.* 0.0025 min^{-1}. **Fig. 13(b)** shows more details of this trend with the individual $k_{loss\text{-}n}$'s for $n = 1–3$. It seems that the decrease in $k_{loss\text{-}ave,0}$ by SiO_2 is fully due to that of $k_{loss\text{-}1}$, while neither of $k_{loss\text{-}2}$ nor $k_{loss\text{-}3}$ is influenced by f_{SiO2}. Though not shown in the figure, the same trends as this were confirmed regardless of char conversion. Taken together with the SiO_2 effect on $k_{Cn,0}$ (**Fig. 11**), that on $k_{loss\text{-}n}$ indicates that the SiO_2 affected the catalytic activity and deactivation kinetics by influencing mainly and selectively those of C1 (i.e., k_{C1} and $k_{loss\text{-}1}$), which was the major catalytic component. It is, however, believed that the decrease in $k_{loss\text{-}1}$ was never due to the C1 deactivation by its irreversible reaction with SiO_2. If the deactivation of C1 was caused mainly by its reaction with SiO_2, $k_{loss\text{-}1}$ could be increased by increasing f_{SiO2}.

Fig. 13(c) shows a good linear relationship between ICA-1 and $k_{\text{loss-ave},0}$, indicating that more active catalyst underwent more rapid deactivation. This is reasonably explained by that C1 was deactivated following not a mechanism of silicate formation but that of self-deactivation through transformation of active nano-sized particles to coarser ones with much lower activity [20]. Linear relationships between the initial activity and rate constant for deactivation of catalyst were reported by the present authors [12,14,15]. It is reasonably concluded from the results shown in **Figs. 11 and 13** that SiO_2 was not necessarily involved in the catalyst deactivation 'during' the gasification.

As already demonstrated, the SiO_2 deactivated the C1 and C1prec until the beginning of gasification. This is explained well by the formation of Na- and Ca-silicates that are favored thermodynamically over the temperature of interest. On the other hand, there was no evidence supporting progress of such chemical events during the gasification. The main difference between 'before' and 'during' the gasification was, without saying, the CO_2 richness of the atmosphere. It is believed that the catalyst deactivation due to silicate formation was chemically inhibited, while the progress of gasification increased both the catalyst and SiO_2 concentrations in the coke increasing the frequency of their contact. The CO_2 gasification is catalyzed by either of the following two different types of redox cycles.

Metal-oxide cycles:

$2Na + CO_2 = CO + Na_2O$ (ΔG = –80 kJ/mol at 900°C)

and then $Na_2O + C = CO + 2Na$ (+46)

$Ca + CO_2 = CO + CaO$ (–331)

and then $CaO + C = CO + Ca$ (+297)

Oxide-carbonate cycles:

$Na_2O + CO_2 = Na_2CO_3$ (–143)

and then $Na_2CO_3 + C = 2CO + Na_2O$ (+109)

$CaO + CO_2 = CaCO_3$ (+10),

and then $CaCO_3 + C = 2CO + CaO$ (–44)

Each cycle consists of reactions with $\Delta G > 0$ and $\Delta G < 0$. On the other hand, all of the reactions of the Na/Ca oxides and carbonates with SiO_2 to form silicates have $\Delta G < 0$, as follows.

$Na_2O + SiO_2 = Na_2SiO_3$ (–225)

$Na_2CO_3 + SiO_2 = Na_2SiO_3 + CO_2$ (–82)

$CaO + SiO_2 = CaSiO_3$ (–88)

$CaCO_3 + SiO_2 = CaSiO_3 + CO_2$ (–98)

It is thus suggested that the above-mentioned catalytic reaction cycles prevented Na/Ca oxides/carbonate from converted into the silicates kinetically rather than thermodynamically.

2.4. Conclusions

This work investigated the effect of SiO_2 that was dispersed in the carbonaceous matrix of coke on the kinetics of its CO_2 gasification with a particular focus on the deactivation of the inherent metallic species, and has drawn the following conclusions within the range of the experimental conditions.

(1) The kinetic model describes the time-dependent change in the coke conversion quantitatively over the range of 0–0.999 by assuming the presence of four different types of catalysts (C1–C4) with different initial activities and deactivation kinetics, and in addition, the precursor of C1 (C1prec).

(2) The SiO_2 deactivates a substantial portion of C1 and entire portion of C1prec before the gasification, i.e., during the pyrolysis/carbonization of briquette. The blending SiO_2

beyond f_{SiO2} = 9.2 wt%-briquette is ineffective for further progress of deactivation and slowdown of gasification.

(3) The catalysts undergo deactivation obeying a self-deactivation mechanism rather than by reactions with SiO_2, and therefore the rate of catalyst deactivation is correlated very well and linearly with the initial catalyst activity.

References

[1] K. Miura, J.-J. Xu, Y. Tezen, H. Nagai, K. Hashimoto, Gasification reactivity of various demineralized coals, *Nenryokyokaishi*, **66** (1987) 264–272. (in Japanese)

[2] K. Miura, K. Hashimoto, P. L. Silveston, Factors affecting the reactivity of coal chars during gasification, and indices representing reactivity, *Fuel* **68** (1989) 1461–1475.

[3] A. Tomita, Y. Ohtsuka, Chapter 5 - Gasification and Combustion of Brown Coal, in: C.-Z. Li (Eds.), Advances in the Science of Victorian Brown Coal, Elsevier, Amsterdam, 2004, pp. 223–285. DOI: 10.1016/B978-008044269-3/50006-6.

[4] J-i. Hayashi, K. Miura, Chapter 4 - Pyrolysis of Victorian brown coal, in: C.-Z. Li (Eds.), Advances in the Science of Victorian Brown Coal, Elsevier, Amsterdam, 2004, pp. 134–222. DOI: 10.1016/B978-008044269-3/50005-4.

[5] A. Mori, S. Kubo, S. Kudo, K. Norinaga, T. Kanai, H. Aoki, J.-i. Hayashi, Preparation of high-strength coke by carbonization of hot-briquetted Victorian brown coal, *Energy Fuels* **26** (2012) 296–301.

[6] A. Mori, M. D. Yuniati, A. T. Mursito, S. Kudo, K. Norinaga, M. Nonaka, T. Hirajima, H.-S. Kim, J.-i. Hayashi, Preparation of coke from Indonesian lignites by a sequence of hydrothermal treatment, hot briquetting, and carbonization, *Energy Fuels* **27** (2013) 6607–6616.

[7] Karnowo, S. Kudo, Aska Mori, Z. F. Zahara, K. Norinaga, J.-i. Hayashi, Modification of reactivity and strength of formed coke from Victorian lignite by leaching of metallic species, *ISIJ Int.*, **55** (2015) 765–774.

[8] M. Naito, A. Okamoto, K. Yamaguchi, T. Yamaguchi, Y. Inoue, Improvement of blast furnace reaction efficiency by use of high reactivity coke, *Tetsu-to-Hagane*, **87** (2001) 357–364. (in Japanese)

[9] J. N. Knudsen, P. A. Jensen, K. Dam-Johansen, Transformation and release to the gas phase of Cl, K, and S during combustion of annual biomass, *Energy Fuels* **18** (2004) 1385–1399.

[10] P. A. Jensen, F. J. Frandsen, K. Dam-Johansen, B. Sander, Experimental investigation of the transformation and release to gas phase of potassium and chlorine during straw pyrolysis, *Energy Fuels* **14** (2000) 1280–1285.

[11] T. Okuno, N. Sonoyama, J.-i. Hayashi, C.-Z. Li, C. Sathe, T. Chiba, Primary release of alkali and alkaline earth metallic species during the pyrolysis of pulverized biomass, *Energy Fuels* **19** (2005) 2164–2171.

[12] E. Byambajav., Y. Hachiyama, S. Kudo, K. Norinaga, J.-i. Hayashi, Kinetics and mechanism of CO_2 gasification of chars from 11 Mongolian lignites, *Energy Fuels* **30** (2016) 1636–1646.

[13] M. Kajita, T. Kimura, K. Norinaga, C.-Z. Li, J.-i. Hayashi, Catalytic and noncatalytic mechanisms in steam gasification of char from the pyrolysis of biomass, *Energy Fuels* **24** (2010) 108–116.

[14] T. Kitsuka, B. Bazardorj, N. Sonoyama, S. Hosokai, C.-Z. Li, K. Norinaga, J.-i. Hayashi, Behavior of inherent metallic species as a crucial factor for kinetics of steam gasification of char from coal pyrolysis, *Energy Fuels* **21** (2007) 387–394.

[15] Z. F. Zahara, S. Kudo, Daniyanto, U. P. M. Ashik, K. Norinaga, A. Budiman, J.-i. Hayashi, CO_2 gasification of sugar cane bagasse: quantitative understanding of kinetics and catalytic roles of inherent metallic species, *Energy Fuels* **32** (2018) 4255–4268.

[16] M. Sugano, K. Mashimo, T. Wainai, Structural changes of lower rank coals by cation exchange, *Fuel* **78** (1999) 945–951.

[17] Q. Liu, H. Hu, Q. Zhou, S. Zhu, G. Chen, Effect of inorganic matter on reactivity and kinetics of coal pyrolysis, *Fuel* **83** (2004) 713–718.

[18] S. Kudo, Y. Hachiyama, H.-S. Kim, K. Norinaga, J.-i. Hayashi, Examination of kinetics of non-catalytic steam gasification of biomass/lignite chars and its relationship with the variation of the pore structure, *Energy Fuels* **28** (2014) 5902–5908.

[19] H. Wu, J.-i. Hayashi, T. Chiba, T. Takarada, C.-Z. Li, Volatilisation and catalytic effects of alkali and alkaline earth metallic species during the pyrolysis and gasification of

Victorian brown coal. Part V. Combined effects of Na concentration and char structure on char reactivity, Fuel **83** (2004) 23–30.

[20] H.-S. Kim, S. Kudo, K. Tahara, Y. Hachiyama, H. Yang, K. Norinaga, J.-i. Hayashi, Detailed kinetic analysis and modeling of steam gasification of char from Ca-loaded lignite, *Energy Fuels* **27** (2013) 6617–6631.

Table 1. Kinetic parameters optimized through kinetic analysis.

f_{SiO2}, wt%	0	4.6	9.2	13.7
k_{nc}, min^{-1}	$2.1 \cdot 10^{-3}$	$2.1 \cdot 10^{-3}$	$2.1 \cdot 10^{-3}$	$2.1 \cdot 10^{-3}$
ICA-1, min^{-1}	$9.1 \cdot 10^{-3}$	$5.9 \cdot 10^{-3}$	$4.8 \cdot 10^{-3}$	$5.5 \cdot 10^{-3}$
ICA-2, min^{-1}	$2.5 \cdot 10^{-2}$	$7.5 \cdot 10^{-3}$	$5.5 \cdot 10^{-3}$	$5.5 \cdot 10^{-3}$
$k_{loss\text{-}ave,0}$, min^{-1}	$5.2 \cdot 10^{-3}$	$3.2 \cdot 10^{-3}$	$2.5 \cdot 10^{-3}$	$2.9 \cdot 10^{-3}$
C_{C1prec}, -	$6.4 \cdot 10^{-1}$	$2.2 \cdot 10^{-1}$	$1.2 \cdot 10^{-1}$	0
$C_{C1,0}$, -	$2.7 \cdot 10^{-1}$	$5.2 \cdot 10^{-1}$	$5.8 \cdot 10^{-1}$	$6.8 \cdot 10^{-1}$
$C_{C2,0,-}$	$6.0 \cdot 10^{-2}$	$2.0 \cdot 10^{-1}$	$2.3 \cdot 10^{-1}$	$2.5 \cdot 10^{-1}$
$C_{C3,0,-}$	$2.9 \cdot 10^{-2}$	$5.5 \cdot 10^{-2}$	$6.3 \cdot 10^{-2}$	$6.4 \cdot 10^{-2}$
$C_{C4,0,-}$	$6.0 \cdot 10^{-3}$	$5.5 \cdot 10^{-3}$	$6.9 \cdot 10^{-3}$	$7.8 \cdot 10^{-3}$
k_{C1prec}, min^{-1}	$1.3 \cdot 10^{-2}$	$2.0 \cdot 10^{-2}$	$3.0 \cdot 10^{-2}$	-
$k_{C1,0}$, min^{-1}	$6.7 \cdot 10^{-3}$	$3.9 \cdot 10^{-3}$	$3.2 \cdot 10^{-3}$	$3.7 \cdot 10^{-3}$
$k_{C2,0}$, min^{-1}	$1.5 \cdot 10^{-3}$	$1.5 \cdot 10^{-3}$	$1.3 \cdot 10^{-3}$	$1.4 \cdot 10^{-3}$
$k_{C3,0}$, min^{-1}	$7.3 \cdot 10^{-4}$	$4.1 \cdot 10^{-4}$	$3.5 \cdot 10^{-4}$	$3.5 \cdot 10^{-4}$
$k_{C4,0}$, min^{-1}	$1.5 \cdot 10^{-4}$	$4.1 \cdot 10^{-5}$	$3.8 \cdot 10^{-5}$	$4.3 \cdot 10^{-5}$
$k_{1oss\text{-}1}$, min^{-1}	$6.8 \cdot 10^{-3}$	$4.3 \cdot 10^{-3}$	$3.2 \cdot 10^{-3}$	$3.8 \cdot 10^{-3}$
$k_{1oss\text{-}2}$, min^{-1}	$9.0 \cdot 10^{-4}$	$1.3 \cdot 10^{-3}$	$1.3 \cdot 10^{-3}$	$1.2 \cdot 10^{-3}$
$k_{1oss\text{-}3}$, min^{-1}	$2.0 \cdot 10^{-4}$	$2.2 \cdot 10^{-4}$	$1.9 \cdot 10^{-4}$	$2.0 \cdot 10^{-4}$
$k_{1oss\text{-}4}$, min^{-1}	$1.0 \cdot 10^{-7}$	$1.0 \cdot 10^{-5}$	$1.8 \cdot 10^{-6}$	$1.0 \cdot 10^{-7}$

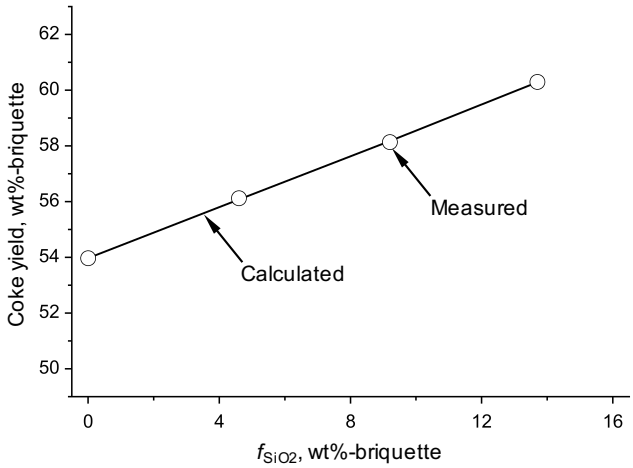

Fig. 1. Effect of f_{SiO2} on coke yield. Plot; measured yield, solid and straight line; calculated yield.

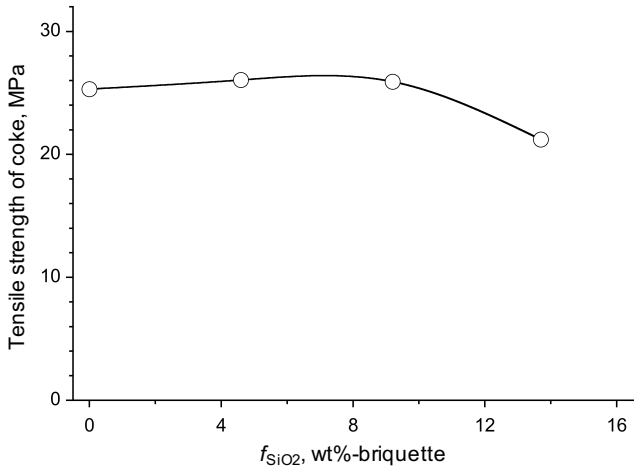

Fig. 2. Effect of f_{SiO2} on tensile strength of coke.

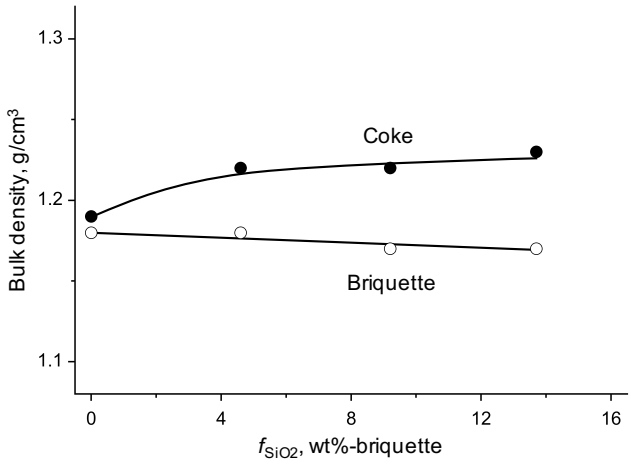

Fig. 3. Effects of f_{SiO2} on bulk densities of briquette and coke.

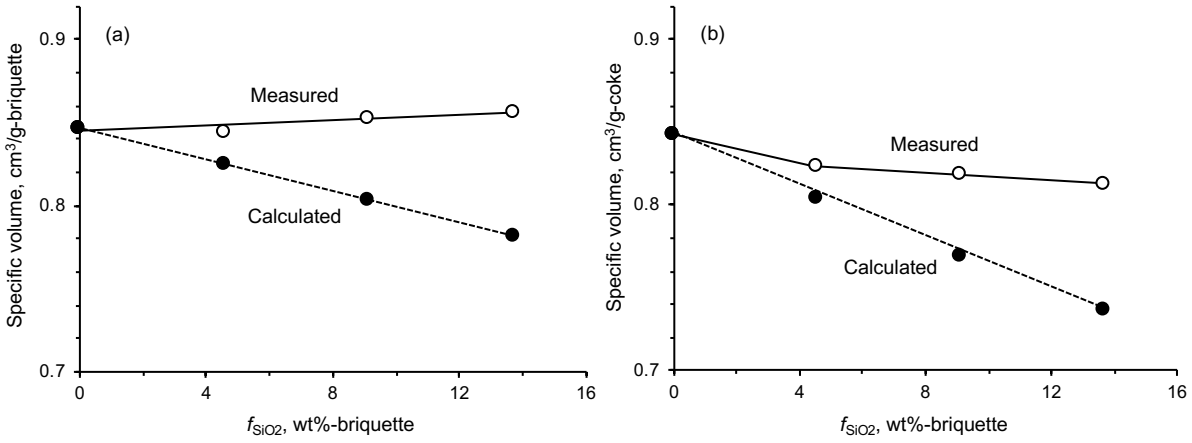

Fig. 4. Effect of f_{SiO2} on specific volume of (a) briquette and (b) coke.

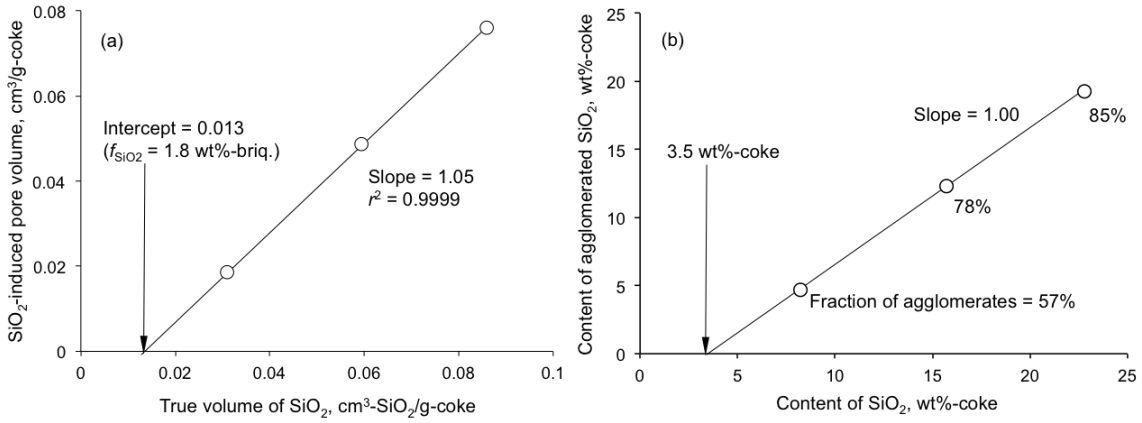

Fig. 5. (a) Plot of SiO_2-induced pore volume against true volume of SiO_2, (b) Plot of estimated content of agglomerated SiO_2 against total SiO_2 content in coke.

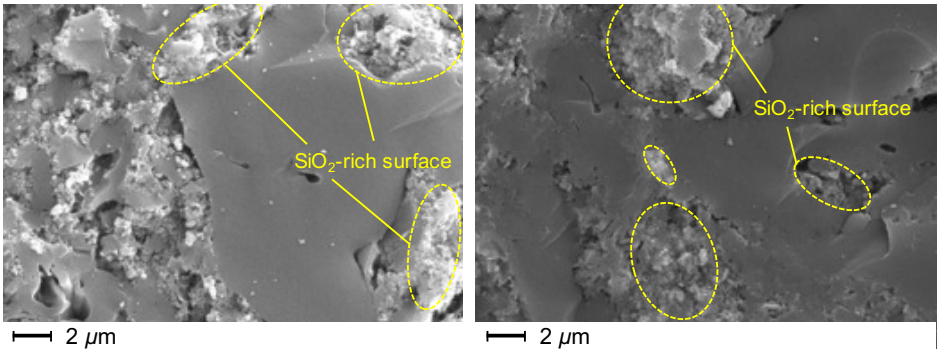

Fig. 6. SEM photographs of fractured surfaces of coke from SiO_2-blended lignite with f_{SiO2} = 9.2 wt%. Bright areas indicated by circles are attributed to SiO_2 or SiO_2-rich parts of the surface.

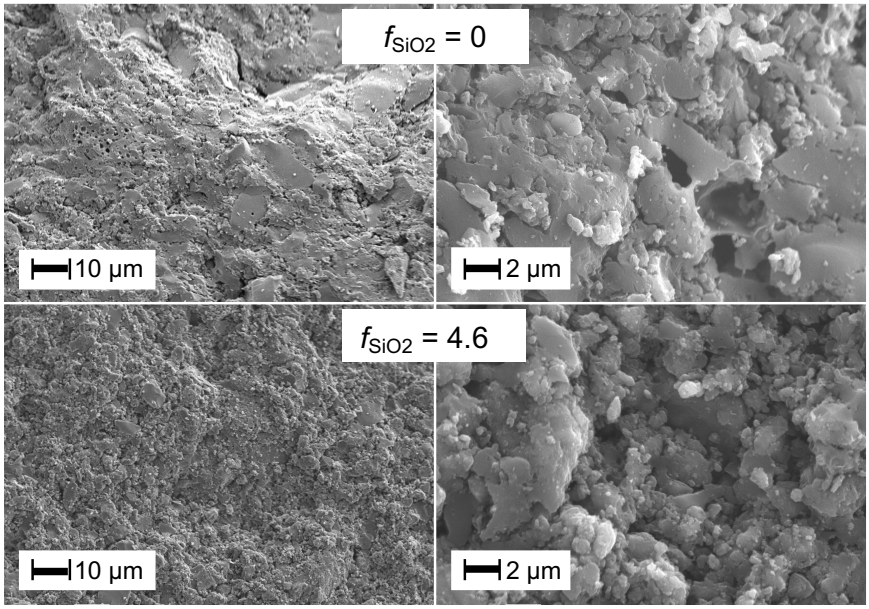

Fig. 7. SEM photographs of fractured surfaces of coke from lignite (f_{SiO2} = 0) and that from SiO_2-blended lignite with f_{SiO2} = 4.6 wt%.

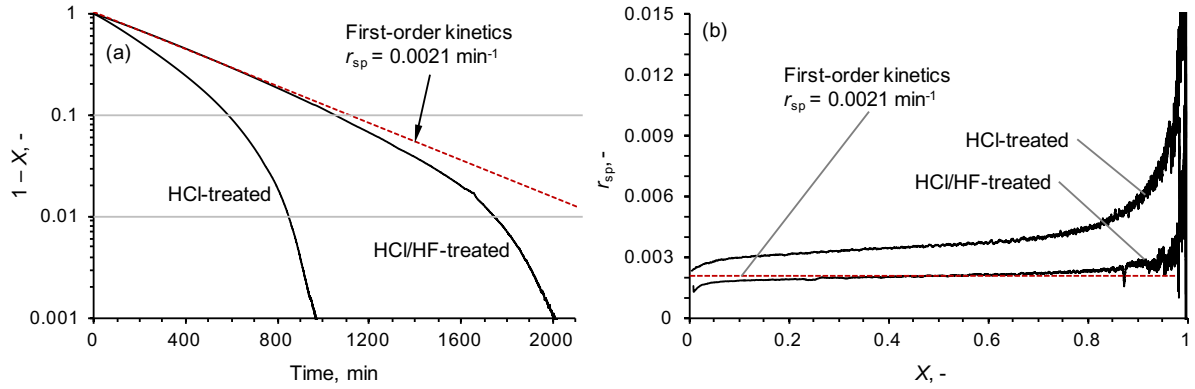

Fig. 8. (a) Time-dependent change in the unconverted fraction (1–*X*) of cokes from HCl/HF-treated lignite and HCl-treated lignite. The dashed line indicates first-order kinetics, i.e., $dX/dt = 0.0021\ (1–X)$. (b) Specific rates of gasification, $r_{sp} = dX/dt/(1–X)$, as functions of coke conversion (*X*).

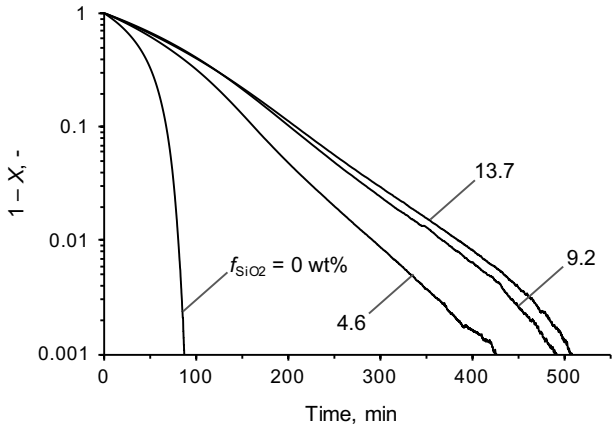

Fig. 9. Time-dependent changes in the residual mass fraction of coke (1–*X*).

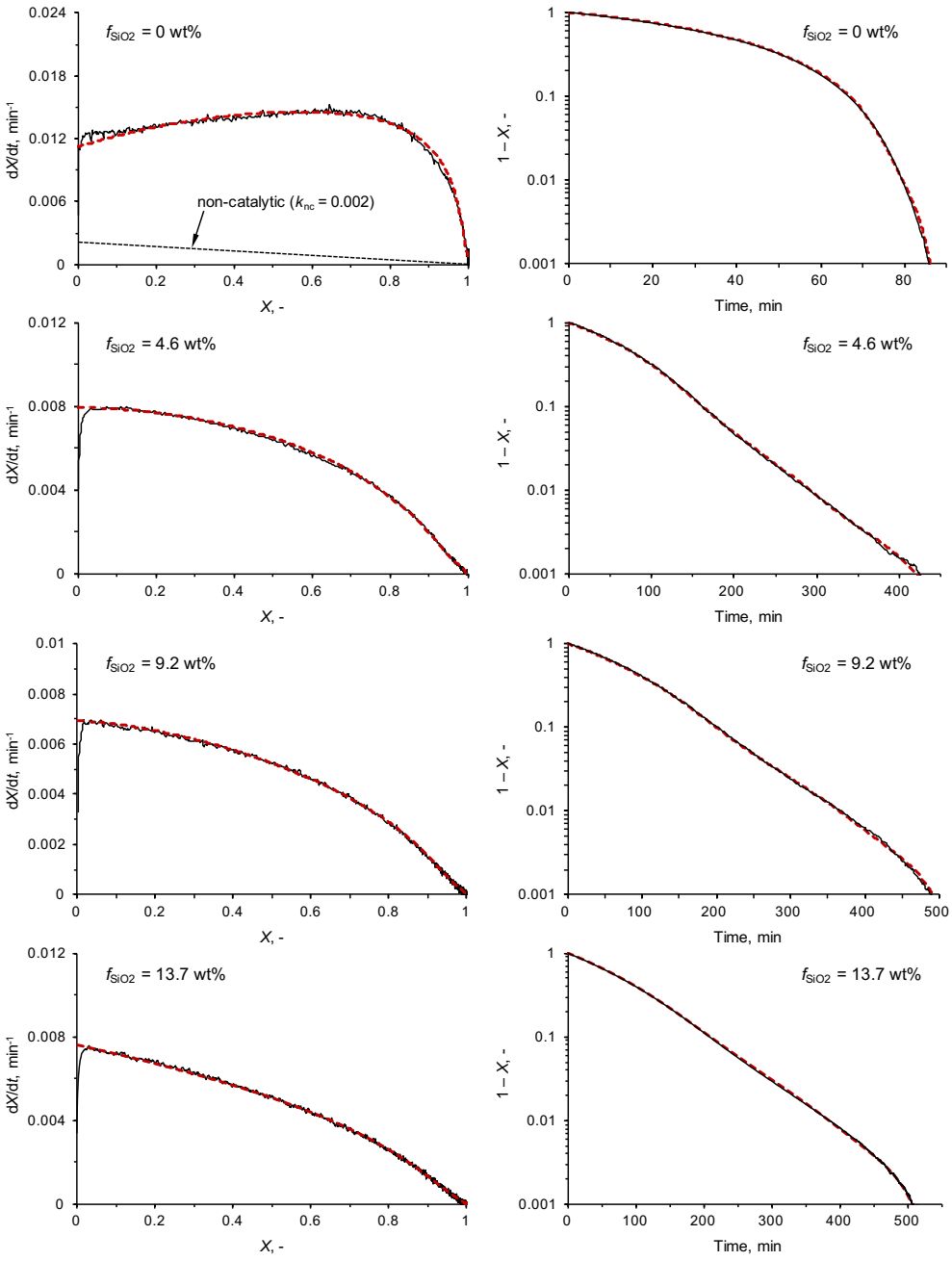

Fig. 10. Measured and calculated rate of gasification (*dX/dt*) over the entire range of conversion (left) and time-dependent changes in the unconverted fraction (1–*X*) (right) for cokes with different f_{SiO2}. The black-colored solid line: measured *dX/dt* or 1–*X*. The black-colored dashed line: the non-catalytic part of *dX/dt* given by k_{nc} = 0.0021 min^{-1}. The red-colored dashed lines: *dX/dt* or 1–*X* calculated by the model.

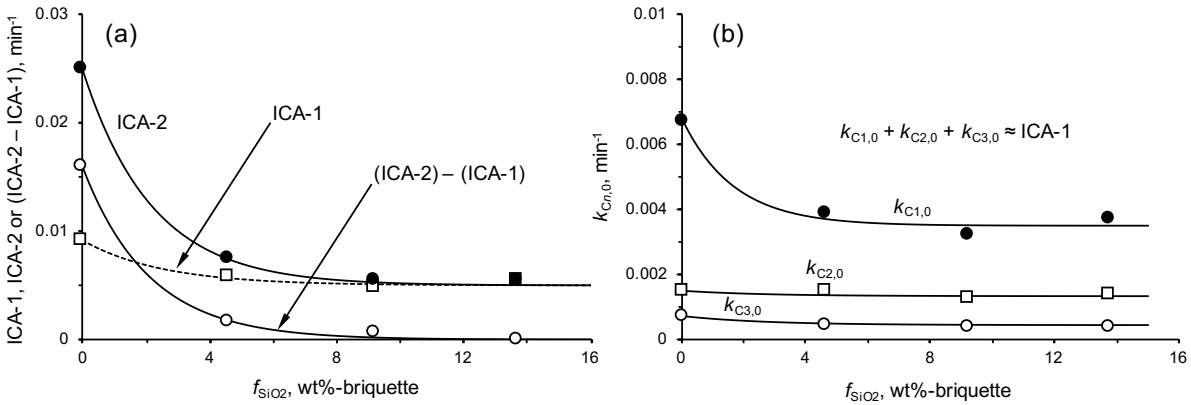

Fig. 11. Effects of f_{SiO2} on the overall and individual catalytic activities.

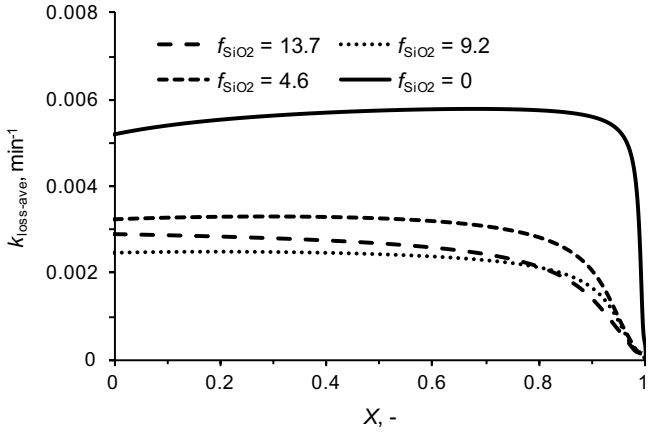

Fig. 12. Change in averaged rate constant for catalyst deactivation ($k_{loss-ave}$) with coke conversion.

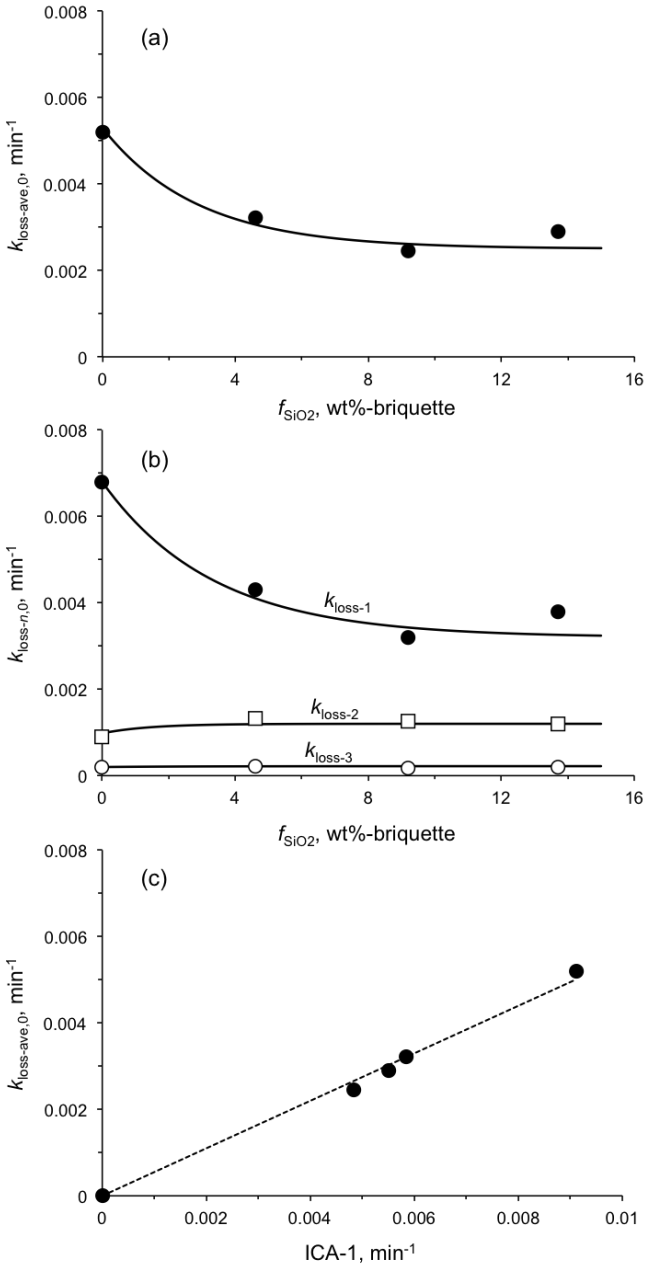

Fig. 13. Effects of f_{SiO2} on (a) initial $k_{loss\text{-}ave}$ and (b) initial $k_{loss\text{-}n}$ (n = 1–3), and (c) that of the initial catalytic activity (ICA) on initial $k_{loss\text{-}ave}$.

Chapter 3

Kinetics and Mechanism of Decomposition of Benzene over Lignite Char

3.1. Introduction

Elimination of tar (i.e., aromatic compounds) has been an important technical issue of gasification of coal and biomass operated at temperature lower than 1000°C. It is recognized that use of char is a most effective way to eliminate the tar, as reviewed by Devi *et al*. [1], Abu El-Rub *et al*. [2], Li [3] and Hayashi *et al*. [4]. Ability of char to enhance the tar decomposition was first reported by Chembukulam *et al*. [5], who showed near complete decomposition of tar from the pyrolysis of woody biomass within a charcoal bed at 950°C. Such effectiveness of using charcoal was demonstrated for continuous gasification of woody biomass by Brandt *et al*. [6]. Extensive decomposition of tar was also reported by Hayashi *et al*. [7] and Iwatsuki *et al*. [8], who performed lignite pyrolysis in drop-tube reactors with continuous co-feeding of steam and the pulverized lignite, and found simultaneous and rapid progress of steam gasification of nascent char and decomposition of nascent tar over the char at temperature of 800–900°C. Then, many researchers reported reduction of tar concentration in the product gas by employing char from coal or biomass with varieties of reactors, atmospheres, temperatures and fuel types [9-27].

Mechanism and kinetics of tar decomposition on char surface have been studied [28-35]. Hosokai *et al*. [28] investigated decomposition of model compounds (mono- to tetra-aromatic hydrocarbons and phenol) over a wood char in the presence/absence of steam and H_2 in the atmosphere. Among the aromatics employed, benzene and naphthalene were the most and second most refractory. In the absence of steam, the char activity (represented by once-through conversion of aromatics) was lost by accumulation of deposited carbon in/on the porous system of the char, in other words, consumption of pores. They claimed that 'consumptive' micropores (size < 1.5 nm) were responsible for the activity while estimated

that mesopores played a role of introducing vapor into micropores. They also found that the char activity was maintained if the steam gasification (micropore creation) occurred at a carbon-based rate equivalent with or greater than that of carbon deposition (micropore consumption).

Kinetics of decomposition of aromatic compounds over char was also investigated by other research groups [29-35]. A common conclusion from those studies was that the activation (gasification) of the char greatly enhances its activity making it more durable. The researchers also made a focal point on a particular behavior of the char, that is, deactivation due to loss of micropores [28,33] or mesopores [35]. Fuentes-Cano et al. [34] reported that the char activities toward naphthalene and toluene decreased with time in the absence of steam (i.e., under pyrolytic conditions) and also in its presence at concentration insufficiently high for fast char gasification *in-situ* recuperating it. The conversion of aromatics decreased to a level equivalent to that for a reference material (SiC), suggesting complete or near-complete deactivation of the char. Fuentes-Cano *et al*. [35] also performed decomposition of naphthalene over pre-activated chars under pyrolytic conditions, and found that the naphthalene conversion decreased and then became near stable within a certain range (20–60%). Similar trends were reported by Burhenne and Aicher [32] who showed time-dependent changes in the activities of pre-activated chars toward benzene. Nestler *et al*. [33] investigated the decomposition of naphthalene over non-activated chars and activated ones. They reported that the activity of a non-activated char was lost quickly and completely or near completely at 850°C while another char lost its activity more slowly and not completely.

In view of the above, it is hypothesized that both pre-activated and non-activated chars lose its activity, unless the gasification occurs *in-situ* at a sufficient rate, but not completely, leaving a certain level of activity, in other words, the char has two different modes of activities. This was a motivation of this work. Another motivation was necessity of further improvement of the experimental system. The previous reactors and operating conditions were not necessarily optimized for monitoring the char activity that can greatly change over ranges from full conversion of aromatics to near zero. Those reactors were not necessarily ‘differential’ reactors, rather, ‘integral’ ones with gas residence times of 50–200

ms (except some examples [32]). Such residence time could be too long to derive kinetics of aromatics decomposition correctly. Such long residence time could also vary the composition of gaseous species and the activity of char along the bed axis. Intermittent measurement of conversion of aromatics with long intervals could miss quick change in the char activity, in particular, very early and quick deactivation.

This work primarily aimed to continuously measure the char activity for benzene decomposition under pyrolytic condition over the entire range up to complete loss of the activity as a function of amount of carbon deposit as well as time, expecting critical examination of the above-described hypothesis. For accomplishing this purpose, the authors developed a new measurement system that consisted of a micro fixed bed of char, a flame ionization detector, as well as benzene vapor generator and distribution lines. Continuous measurements were combined with intermittent and batch analyses of light gases, benzene (feed) and lighter/heavier products.

3.2. Experimental

3.2.1. Material

Three different chars were prepared and used. The lignite sample was prepared from a Victorian lignite, Loy Yang, which was dried partially leaving some moisture (ca. 10 wt%) and pulverized to sizes smaller than 106 μm prior to use. A char sample (Char-1) was prepared by pyrolyzing the lignite in atmospheric flow of N_2 with heating rate and peak temperature of 10 °C/min and 900°C, respectively. The contents of metallic species of Char-1 were as follows: Na; 0.15, K; 0.009, Mg; 0.13, Ca; 0.097 wt%-char. The lignite sample was also subjected to sequential acid treatments in aqueous solutions of HCl (3 mol/L), HF (3 mol/L) and then HCl (3 mol/L) for removal of major metallic species (Na, Ca, Mg, and Fe), Si- and Al-containing species. The acid-washed lignite, of which the contents of Na, K, Mg, and Ca were respectively 0.00027, 0.00026, 0.00048, and 0.0018 wt%-coal, was pyrolyzed under the same conditions as above. The resulting char is hereafter referred to as Char-2. This char was gasified with CO_2 up to a mass-based conversion of 60%. Temperature and

atmosphere were 900°C and an equimolar CO_2/N_2 mixture, respectively. The partially gasified Char-2 is termed Char-3. All of the char samples were sieved to collect fraction with particle sizes of 38–75 μm, and then used for experiments. The char samples were subjected to N_2 adsorption/desorption at –196°C with an analyzer (Quantachrome Instruments, model Autosorb®-iQ). **Table 1** shows properties of the char samples relevant to their porous natures. Benzene of a guaranteed reagent grade (Wako Chemicals Co., Japan) was chosen as a model compound of tar, and used without further purification.

3.2.2. Continuous monitoring of benzene decomposition over char

Fig. 1 shows a schematic diagram of the apparatus. It consists of three main components (vaporizer, reactor and flame ionization detector (FID)) and controllers and parts. An asymmetrical U-shaped tube is used as the vertical reactor. It is made of transparent quartz glass with inner diameters of 6.0 and 4.0 mm at the inlet and outlet sides, respectively. The reactor is packed with a bed of char particles (mass of char; 20 mg, bed height; 1.8 mm, bulk density; 0.40 g/cm^3), which is fixed at near-bottom of the upstream part.

The benzene vaporizer consists of a cylindrical glass bottle with a volume of 50 ml. The primary carrier gas (N_2, purity > 99.9996 vol%) is continuously introduced into the headspace of the bottle at a rate of 20 ml/min (at 1.0 atm and 25°C), where benzene is vaporized at a steady rate. The benzene vapor is diluted by the secondary N_2 (80 ml/min) to a concentration within a range of approximately 1,100–1600 ppmv (3.8–5.6 g-benzene/Nm^3), and then fed into the reactor for a prescribed period of time (30–120 min). The benzene concentration is controlled by varying the temperature of the vaporizer. The gas residence time within the char bed is calculated as 7.6 ms on an empty basis at 900°C. The near-entire portion of the exit gas (except a very small portion for intermittent sampling) is introduced continuously into the FID that detects benzene (unconverted) and the other hydrocarbon species, if any, together. The FID response is monitored and recorded continuously. During the feeding of benzene vapor into the reactor, small portions of gas (0.4-ml for each) are sampled at the reactor upstream and downstream intermittently and analyzed with a gas chromatograph (Shimadzu, model GC-14B) that is equipped with an FID and columns for

gas separation and CO/CO_2 methanation. The conversion on benzene was determined directly by its concentrations upstream/downstream the reactor. This made possible to quantify the downstream concentration continuously from the FID response.

Table 2 lists the conditions for the individual blank tests without char bed (B) and runs with char bed (R). Three runs, B1.3, R2.5 and R4.4, were performed exclusively for collecting the condensable organic matter (benzene and heavier aromatics) completely at the reactor downstream, and analyzing the composition by gas-chromatography mass spectrometry (GC/MS) on a Perkin Elmer model, Clarus SQ8.

Fig. 2(a) shows the FID responses during a sequence of blank tests, B1.1 and B1.2, without char bed. The horizontal axis indicates the time elapsed since the switching of the 4-way valve (see **Fig. 1**) to start supply of benzene vapor to the reactor. Each FID signal occurs around 0.1 min, which is time required for the gas to travel between the 4-way valve and the FID (see **Fig. 1**). Then, the intensity increases steeply and becomes steady within 0.8 min. The shapes of the curves are different from those for 'ideal' step responses, and this is believed to be due to unavoidable back mixing of the gas. It is more importantly noted that the signal profiles in the two tests are highly reproducible. Each signal is arisen from not only benzene but also other hydrocarbons if formed in the reactor. It was confirmed in a test (B1.3) that benzene conversion in the gas phase was steady at 0.45% on carbon basis giving two aromatic compounds (biphenyl; 0.43%, naphthalene 0.02%) while neither light hydrocarbons such as CH_4 nor soot was detected. **Fig. 2(b)** shows the results from a sequence of R1.1 and R1.2 with high reproducibility of the FID response. Benzene was not decomposed at all even at 700°C in the presence of Char-1. It was thus confirmed that the FID response was reproducible unless benzene underwent decomposition over the char.

3.3. Results and Discussion

3.3.1. Decomposition of benzene on Char-3

Fig. 3 shows the FID responses in a sequence of two runs with Char-3, i.e., R4.1 and R4.2. In the former run, the FID signal intensity increases gradually and becomes steady at

36 min. It is also seen that the signal intensity after 36 min is slightly but systematically lower than 100% that corresponds to no benzene conversion. In R4.2 with the spent Char-3 from R4.1, the signal intensity is steady over the period of benzene feeding and at the same level as that at 36–50 min in R4.1. Though not shown, the signal intensity at 97% was maintained in the following run (R4.3, 80 min). This result indicates that Char-3 had two different types of surfaces. One was *very active but consumptive*, and the other was *less active but non-consumptive*. These are hereafter referred to as *Type I* and *Type II surfaces*, respectively.

Fig. 4 exhibits the difference in the FID intensity between R4.1 and R4.2 as a function of time. The vertical axis means the benzene conversion into carbon (C) deposit on Type I surface. The initial conversion is around 70%, which corresponds to a first-order rate constant as high as 160 s^{-1}. The rate constant, k, is hereafter expressed by the first-order rate equation ($\frac{dX}{dt} = k(1 - X)$, where, X and t represent the benzene conversion into C deposit and the time exposed to benzene vapor, respectively). Within the interval of 0–36 min in R4.1, no carbon deposit was detected at either the upstream or downstream of the char bed, and it is therefore judged that the benzene conversion shown in **Fig. 4** is equivalent to that into C deposit onto Type I surface of Char-3. In R4.4 with fresh Char-3 and benzene feeding time of 30 min, biphenyl and naphthalene were recovered at the reactor downstream. Their respective yields, 0.41% and 0.02%, were almost the same as those in B1.3 (0.43% and 0.02%, respectively). It was believed that these diaromatic compounds were formed in the gas phase at steady rates and probably at downstream of the Char-3 bed in R4.1–R4.3, contributing slightly to the FID signals shown in **Fig. 3**.

Further analysis of the results shown in **Figs. 3** and **4** enables to determine the capacity of Type I surface of Char-3 for the C deposition from benzene. As seen in **Fig. 5**, Type I surface of Char-3 had a capacity as much as 22 wt% of its initial mass. On the other hand, the activity of Type II surface was much lower than that of Type I surface, but its activity was steady over the period of at least 140 min (R4.1–R4.3) with a rate constant of 4.0 s^{-1}. Although not demonstrated, it is estimated that the 'capacity' of Type II surface was *sustainable*. This feature is reasonably understood by considering autocatalytic nature of

carbon deposition over carbon surface. Hosokai *et al*. investigated reforming of tar from the pyrolysis of woody biomass with mesoporous alumina. They reported that the alumina had a high ability to deposit vapor of aromatics onto its own acidic surface, and moreover, C deposit in mesopores further enhanced the carbon deposition increasing the tar removal [36]. Fuentes-Cano *et al*. reported that the activity of a type of char toward naphthalene decreased along with C deposition and then reached a certain level (well above zero) depending on the conditions [35]. Nestler *et al*. reported similar trends for decomposition of naphthalene [33]. The presence of Type I and Type II surfaces is thus consistent with those previous reports.

The specific surface areas (determined by applying QS-DFT) of the fresh Char-3, that after R4.4 (30 min exposure to benzene vapor) and spent Char-3 from R4.3 (cumulative exposure time = 140 min) were 1,730, 740 and 56 m^2/g, respectively. According to **Fig. 4**, Char-3 had lost 90% of the initial activity of Type I surface by 30-min exposure to benzene vapor (with respect to the benzene conversion), while the loss of the specific area was limited to 58%. Thus, the surface area arisen from micropores and mesopores was not a measure, or at least, not a direct measure for the Type I surface activity that greatly changed along with the C deposition. On the other hand, the activity of Type II surface seemed to be independent of the specific surface area, which decreased to *ca.* 1/30 of the initial until the end of R4.3. The characteristics of Type II surface is discussed in more detail in the following section.

3.3.2. Decomposition of benzene on Char-1 and Char-2

Fig. 6 shows the FID responses in the sequence of R2.1 and R2.2 with Char-1. There is difference in the signal intensity between these two runs, although it is much less significant if compared with that between R4.1 and R4.2. Char-1 had much smaller capacity of C deposit as well as much lower initial activity than Char-3. As shown in **Fig. 7**, the initial benzene conversion on Type I surface into C deposit is slightly over 10%. It is also seen that Type I surface loses the activity within 4 min. The capacity of the Type I surface was in fact as small as 0.18 wt% of the initial mass of Char-1, and it was only *ca.* 1/120 of the capacity of Char-3. On the other hand, the benzene conversion into C deposit on Type II surface was steady around 4.3% all through R2.1 to R2.4 (total period of benzene feeding; 260 min).

Thus, Type II surface of Char-1 was slightly more active than that of Char-3. The specific QS-DFT surface areas of the fresh and spent Char-1 were 190 and 17 m^2/g, respectively. Taken together with the steady benzene conversion on Type II surface, it is suspected again that the activity of Type II surface is nearly independent of the micropore/mesopore surface area, at least for the reaction times examined. The above-mentioned steady benzene conversion on Type II surface (4.3%) corresponds to a first-order rate constant of 5.8 s^{-1}. This rate constant means benzene conversion of 0.44 if the residence time is 100 ms. Thus, the activity of Type II surface should not be ignored in a practical sense.

Two phenomena, which had not been reported so far, were found in R2.1 to R2.5. The first one was formation of biphenyl and naphthalene. Their yields were measured in R2.5, and determined as 1.1% and 0.04% on the carbon basis, respectively. These were small but systematically greater than those by the gas-phase reactions of benzene, i.e., 0.43% and 0.02%, respectively. This strongly suggests the formation of those diaromatics on Type II surface, because such diaromatics formation was not detected when Type I surface had sufficiently high activity, as will be mentioned later. It was also found that carbon deposition occurred onto the reactor wall at downstream of the char bed. It was believed that heavier aromatics were formed on Type II surface together with the diaromatics, desorbed from the surface, and then deposited onto the reactor wall. Such heavier aromatics, which was not identified by GC/MS at all, had a high propensity of conversion into C deposit, and therefore could not escape from the reactor.

Fig. 8 shows accumulation of C deposit on Type II surface of Char-1 and that on the reactor wall through R2.1 to 2.4. The linear increases in the amounts of C deposits demonstrate steady activity of Type II surface to form C deposit thereon, diaromatics, and heavier aromatics as the precursor of C deposit on the reactor wall. The above-described results indicate that benzene underwent not only conversion into C deposit but also aromatic ring condensation (and/or polymerization). It is suspected that the same or similar thermochemical events occurred in previous studies, but were missed probably due to the gas residence times within char bed were long enough to prevent heavier aromatics from escaping from the bed.

The activity of Char-2, which was prepared from the acid-washed lignite, was investigated by analyzing the results from R3.1–R3.3. The characteristics of Char-2 was not the same as but similar to those for Char-1, as shown in **Table 3**. Differences in the C deposit yields between Char-1 and Char-2 may be attributed to those in the porous properties and/or the presence of intrinsic metallic species, in particular, Na and Ca that have more or less catalytic activities toward aromatics if dispersed on carbonaceous surface [7,8,34].

3.3.3. Mechanism of benzene decomposition and change in char activity

This section discusses the mechanism of benzene decomposition on the char surface and the change in the char's activity along with the C deposition. Firstly, the char has two different types of surfaces, Type I and Type II, which have clearly different characteristics. Type I surface is initially very active toward benzene, but the activity decreases as the C deposit is accumulated, in other words, consumption of micropores [28,33]. The capacity of Type I surface seems to strongly depend on the initial specific surface area and/or pore volume, as seen in **Fig. 9**. This is clear from comparison of the properties between Char-2 and Char-3 that were prepared from the same parent lignite. Char-3 had initial specific surface area and pore volume greater by *ca.* 9 and 6 times than those of Char-2, respectively, and provided first-order rate constant higher by 15 times. However, it is at present difficult to discuss the change in the surface activity based on the porous properties. As indicated by the point 'A', Char-3 still has a specific surface area and pore volume of 740 m^2/g and 0.41 cm^3/g (42% and 55% of the initials, respectively), where the cumulative amount C deposit has reached *ca.* 99% of the capacity. This indicates that only a part of Type I surface was available for the benzene decomposition. Char-2 has an initial specific pore volume that is about 1/6 of that possessed by Char-3, but the capacity of Char-2 is only 1/170 of the Char-3's capacity.

Fig. 10 shows the pore size distributions of the fresh and spent chars. Exposure of Char-3 to benzene vapor for 30 min decreased the volume of pores with width smaller than 2.0 nm by about a half. However, the remaining pores hardly provided Type I surface. It is estimated that benzene was decomposed forming C deposit filling micropores and also

plugging or narrowing their mouths, preventing benzene vapor from diffusing into 'remaining' those pores. The pore width distribution of the spent Char-3 strongly suggests that those pores were finally closed by further exposure to benzene vapor that was decomposed exclusively on Type II surface. The pores with width of 2–3 nm resulted from the C deposition onto Type II surface. The initial pores of Char-1 and Char-2 with width of 1–2 nm would be narrowed and finally closed in the same way as for Char-3 but much more quickly.

Secondly, Type II surface has characteristics clearly different from Type I surface. Its activity, represented by the benzene conversion or its rate constant, is steady regardless of C deposit accumulation. According to the results from the sequential runs with Char-1, the pathways and fate of benzene are drawn in **Fig. 11**. Benzene chemisorbed onto Type II surface is converted mainly to carbon there and also to diaromatics (mainly biphenyl) and heavier aromatics, which are desorbed from the surface. The heavier aromatics, of which composition is unknown, are further and completely converted to C deposit onto the reactor wall downstream of the char bed. A residence time of benzene vapor as short as 7.6 ms allowed diaromatics and heavier ones to escape from the char bed. A technical subject left for future work is to provide a reactor system that enables to detect and quantify the heavier aromatics minimizing their further conversion into C deposit. From the results shown in **Figs. 9** and **10**, it is speculated that Type II surface arises from macropores into which benzene vapor easily diffuse, therefore providing stable activity even after deposition of substantial amount of carbon.

3.4. Conclusions

This work developed a method to continuously monitor the thermal decomposition of aromatic vapor on the surface of char particles in a form of micro fixed bed, and the following characteristics of benzene decomposition are revealed.

(1) The char provides two different types of surfaces (Types I and II).

(2) Type I surface is very active toward benzene vapor, but the activity is consumptive. The activity is lost along with the C deposition. The CO_2 gasification of Char-2 up to its conversion of 60% increases the initial rate constant of benzene conversion into C deposit and capacity to 15 and 170 times, respectively.

(3) The activity of Type II surface is lower than that of Type I surface, but steady over the time range examined and cumulative amount of C deposit. Benzene undergoes conversion mainly into C deposit but also diaromatics (biphenyl and trace naphthalene) and heavier aromatics, the latter of which escaped the char bed and further converted into C deposit on the reactor wall at downstream.

References

[1] L. Devi, K.J. Ptasinski, F.J.J.G. Jansen, A review of the primary measures for tar elimination in biomass gasification processes, Biomass Bioenergy 24 (2003) 125–140.

[2] Z. Abu El-Rub, E.A. Bramer, G. Brem, Review of Catalysts for Tar Elimination in Biomass Gasification Processes, Ind. Eng. Chem. Res. 43 (2004) 6911–6919.

[3] C.-Z. Li, Some recent advances in the understanding of the pyrolysis and gasification behaviour of Victorian brown coal, Fuel 86 (2007) 1664−1683.

[4] J.-i. Hayashi, S. Kudo, H.-S. Kim, K. Norinaga, K. Matsuoka, S. Hosokai, Low-Temperature Gasification of Biomass and Lignite: Consideration of Key Thermochemical Phenomena, Rearrangement of Reactions, and Reactor Configuration, Energy Fuels 28 (2014) 4−21.

[5] S.K. Chembukulam, A.S. Dandge, N.L. Kovllur, R.K. Seshaglri, R. Valdyeswaran, Smokeless Fuel from Carbonized Sawdust, Ind. Eng. Chem. Prod. Res. Dev. 20 (1981) 714–719.

[6] P. Brandt, E. Larsen, U. Henriksen, High Tar Reduction in a Two-Stage Gasifier, Energy Fuels 14 (2000) 816–819.

[7] J.-i. Hayashi, H. Takahashi, M. Iwatsuki, K. Essaki, A. Tsutsumi, T. Chiba, Rapid conversion of tar and char from pyrolysis of a brown coal by reactions with steam in a drop-tube reactor, Fuel 79 (2000) 439–447.

[8] J.-i. Hayashi, M. Iwatsuki, K. Morishita, A. Tsutsumi, C.-Z. Li, T. Chiba, Roles of inherent metallic species in secondary reactions of tar and char during rapid pyrolysis of brown coals in a drop-tube reactor, Fuel 81 (2002) 1977–1987.

[9] O. Masek, S. Hosokai, K. Norinaga, C.-Z. Li, J.-i. Hayashi, Rapid Gasification of Nascent Char in Steam Atmosphere during the Pyrolysis of Na- and Ca-Ion-Exchanged Brown Coals in a Drop-Tube Reactor, Energy Fuels 23 (2009) 4496−4501.

[10] T. Matsuhara, S. Hosokai, K. Norinaga, K. Matsuoka, C.-Z. Li, J.-i. Hayashi, In-Situ Reforming of Tar from the Rapid Pyrolysis of a Brown Coal over Char Energy Fuels 24 (2010) 76–83.

[11] S. Hosokai, K. Kishimoto, K. Norinaga, C.-Z. Li, J.-i. Hayashi, Characteristics of Gas-Phase Partial Oxidation of Nascent Tar from the Rapid Pyrolysis of Cedar Sawdust at 700-800°C, Energy Fuels 24 (2010) 2900–2909.

[12] X. Zeng, Y. Wang, J. Yu, S. Wu, J. Han, S. Xu, G. Xu, Gas Upgrading in a Downdraft Fixed-Bed Reactor Downstream of a Fluidized-Bed Coal Pyrolyzer, Energy Fuels 25 (2011) 5242–5249.

[13] T. Sueyasu, T. Oike, A. Mori, S. Kudo, K. Norinaga, J.-i. Hayashi, Simultaneous Steam Reforming of Tar and Steam Gasification of Char from the Pyrolysis of Potassium-Loaded Woody Biomass, Energy Fuels 26 (2012) 199–208.

[14] K. Matsuoka, S. Hosokai, K. Kuramoto, Y. Suzuki, Enhancement of coal char gasification using a pyrolyzer–gasifier isolated circulating fluidized bed gasification system, Fuel Process. Tech. 109 (2013) 43–48.

[15] L.-x. Zhang, T. Matsuhara, S. Kudo, J.-i. Hayashi, K. Norinaga, Rapid pyrolysis of brown coal in a drop-tube reactor with co-feeding of char as a promoter of in situ tar reforming, Fuel 112 (2013) 681–686.

[16] T. Oike, S. Kudo, H. Yang, J. Tahara, H.-S. Kim, R. Koto, K. Norinaga, J.-i. Hayashi, Sequential Pyrolysis and Potassium-Catalyzed Steam−Oxygen Gasification of Woody Biomass in a Continuous Two-Stage Reactor, Energy Fuels 28 (2014) 6407−6418.

[17] X. Nitsch, J.-M. Commandré, J. Valette, G. Volle, E. Martin, Conversion of Phenol-Based Tars over Biomass Char under H_2 and H_2O Atmospheres, Energy Fuels 28 (2014) 6936–6940.

[18] Y.-l. Zhang, Y.-h. Luo, W.-g. Wu, S.-h. Zhao, Y.-f. Long, Heterogeneous Cracking Reaction of Tar over Biomass Char, Using Naphthalene as Model Biomass Tar, Energy Fuels 28 (2014) 3129–3137.

[19] Y.-l. Zhang, W.-g. Wu, S.-h. Zhao, Y.-f. Long, Y.-h. Luo, Experimental study on pyrolysis tar removal over rice straw char and inner pore structure evolution of char, Fuel Process. Tech. 134 (2015) 333–344.

[20] H. Yang, S. Kudo, K. Norinaga, J.-i. Hayashi, Steam−Oxygen Gasification of Potassium-Loaded Lignite: Proof of Concept of Type IV Gasification, Energy Fuels 30 (2016) 1616–1627.

[21] Z.-Y. Du, X. Wang, Y.-H. Qin, Z.-H. Zhang, J. Feng, W.-Y. Li, Effects of Secondary Reactions on the Destruction of Cellulose-Derived Volatiles during Biomass/Coal Co-gasification, Energy Fuels 30 (2016) 1145–1153.

[22] X. Zeng, Y. Dong, F. Wang, P. Xu, R. Shao, P. Dong, G. Xu, L. Dong, Fluidized Bed Two-Stage Gasification Process for Clean Fuel Gas Production from Herb Residue: Fundamentals and Demonstration, Energy Fuels 30 (2016) 7277–7283.

[23] D. Feng, Y. Zhao, Y. Zhang, Z. Zhang, H. Che, S. Sun, Experimental comparison of biochar species on in-situ biomass tar H_2O reforming over biochar, Int. J. Hydrog. Energy 42 (2017) 24035–24046.

[24] D. Feng, Y. Zhao, Y. Zhang, S. Sun, Effects of H_2O and CO_2 on the homogeneous conversion and heterogeneous reforming of biomass tar over biochar, Int. J. Hydrog. Energy 42 (2017) 13070–13084.

[25] D. Feng, Y. Zhang, Y. Zhao, S. Sun, J. Gao, Improvement and maintenance of biochar catalytic activity for in-situ biomass tar reforming during pyrolysis and H2O/CO2 gasification, Fuel Process. Tech. 172 (2018) 106–114.

[26] Y. Kawabata, H. Nakagome, T. Wajima, S. Hosokai, H. Sato, K. Matsuoka, Tar Emission during Pyrolysis of Low Rank Coal in a Circulating Fluidized Bed Reactor, Energy Fuels 32 (2018) 1387–1394.

[27] M. Morin, X. Nitsch, M. Hémati, Interactions between char and tar during the steam gasification in a fluidized bed reactor, Fuel 224 (2018) 600–609.

[28] S. Hosokai, K. Kumabe, M. Ohshita, K. Norinaga, C.-Z. Li, J.-i. Hayashi, Mechanism of decomposition of aromatics over charcoal and necessary condition for maintaining its activity, Fuel 87 (2008) 2914–2922.

[29] Z. Abu El-Rub, E.A. Bramer, G. Brem, Experimental comparison of biomass chars with other catalysts for tar reduction, Fuel 87 (2008) 2243–2252.

[30] M. Morgalla, L. Lin, M. Strand, Decomposition of benzene using char aerosol particles dispersed in a high-temperature filter, Energy 118 (2017) 1345–1352.

[31] M. Morgalla, L. Lin, M. Strand, Benzene Conversion in a Packed Bed Loaded with Biomass Char Particles, Energy Fuels 32 (2018) 554–560.

[32] L. Burhenne, T. Aicher, Benzene removal over a fixed bed of wood char: The effect of pyrolysis temperature and activation with CO_2 on the char reactivity, Fuel Process. Tech. 127 (2014) 140–148.

[33] F. Nestler, L. Burhenne, M.J. Amtenbrink, T. Aicher, Catalytic decomposition of biomass tars: The impact of wood char surface characteristics on the catalytic performance for naphthalene removal, Fuel Process. Tech. 145 (2016) 31–41.

[34] D. Fuentes-Cano, A. Gómez-Barea, S. Nilsson, P. Ollero, Decomposition kinetics of model tar compounds over chars with different internal structure to model hot tar removal in biomass gasification, Chem. Eng. J. 228 (2013) 1223–1233.

[35] D. Fuentes-Cano, F. Parrillo, G. Ruoppolo, A. Gómez-Barea, U. Arena, The influence of the char internal structure and composition on heterogeneous conversion of naphthalene, Fuel Process. Tech. 172 (2018) 125–132.

[36] S. Hosokai, J.-i. Hayashi, T. Shimada, Y. Kobayashi, K. Kuramoto, C.-Z. Li, T. Chiba, SPONTANEOUS GENERATION OF TAR DECOMPOSITION PROMOTER IN A BIOMASS STEAM REFORMER, Chem. Eng. Res. Des. 83(A9) (2005) 1093–1102.

Table 1. Porous nature of fresh char. Before exposed to benzene vapor.

Sample	Specific surface area (BET), m^2/g	Specific surface area (QS-DFT[a]), m^2/g	Pore volume (QS-DFT), cm^3/g	Average pore width[b] (QS-DFT), nm
Char-1	205	190	0.15	0.8
Char-2	220	185	0.13	1.4
Char-3	1,890	1,730	0.75	1.3

a. Quenched solid density functional theory. Slit pores were assumed.

b. Slit pores were assumed.

Table 2. Conditions of blank tests (B) and runs (R) with Char-1, Char-2 or Char-3.

ID	Temperature, °C	Bed material	Mass of bed material, mg	Benzene conc. ppmv	Gas flow rate @25°C, cm^3/min	Feeding time, min	Remark
B1.1	900	none	-	1,215	100	30	Benzene feeding was paused between runs, and resumed when FID response became stable.
B1.2		none	-			30	
B1.3	900	none	-	1,140	100	80	Carried out exclusive for recovery/analysis of aromatic products.
R1.1	700	Char-1	20	1,185	100	40	Sequential feeding of benzene to the identical bed of Char-1. Benzene feeding was paused between runs, and resumed when FID response became stable.
R1.2						40	
R2.1	900	Char-1	20	1,245	100	30	Sequential feeding of benzene to the identical bed of Char-1. Benzene feeding was paused among runs, and resumed when FID response became stable.
R2.2				1,245		30	
R2.3				1,245		80	
R2.4				1,290		120	
R2.5	900	spent Char-1 from R2.4	20[a)]	1,525	100	80	Carried out exclusively for recovery of benzene and heavier aromatics products.
R3.1	900	Char-2	20	1,175	100	30	Sequential feeding of benzene to the identical bed of Char-2. Benzene feeding was paused among runs, and resumed when FID response became stable.
R3.2						30	
R3.3						80	
R4.1	900	Char-3	20	1,275	100	50	Sequential feeding of benzene to the identical bed of Char-3. Benzene feeding was paused among runs, and resumed when FID response became stable.
R4.2						50	
R4.3						80	
R4.4	900	spent Char-3 from R4.3	20	1,165	100	30	Carried out exclusively for recovery of benzene and heavier aromatics products.

a) The entire portion of the spent Char-1 from R2.4 was used.

Table 3. Comparison of properties of Char-1 and Char-2 relevant to activity for benzene decomposition.

Sample	Char-1	Char-2
Initial benzene conversion on Type I surface, %	11	8.0
(first-order rate constant, s^{-1})	(15)	(11)
Capacity of Type I surface (amt. of C deposit), wt%-char	0.18	0.13
Steady-state benzene conversion to C deposit on Type II surface, %	3.9	3.9
(first-order rate constant, s^{-1})	(5.3)	(5.4)
Steady-state benzene conversion to C deposit on reactor wall, %	0.38	0.07

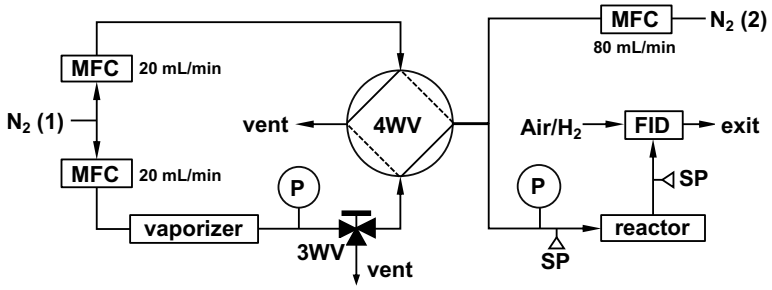

Fig. 1. Schematic diagram of experimental system. 3WV and 4WV; 3-way and 4-way valves, respectively, FID; flame ionization detector (originally installed in a gas chromatograph, Shimadzu Co. Ltd, model GC-14B), MFC; mass flow controller, N_2 (1) and N_2 (2); primary and secondary carrier gases, respectively, P; pressure monitor, SP; gas/vapor sampling port.

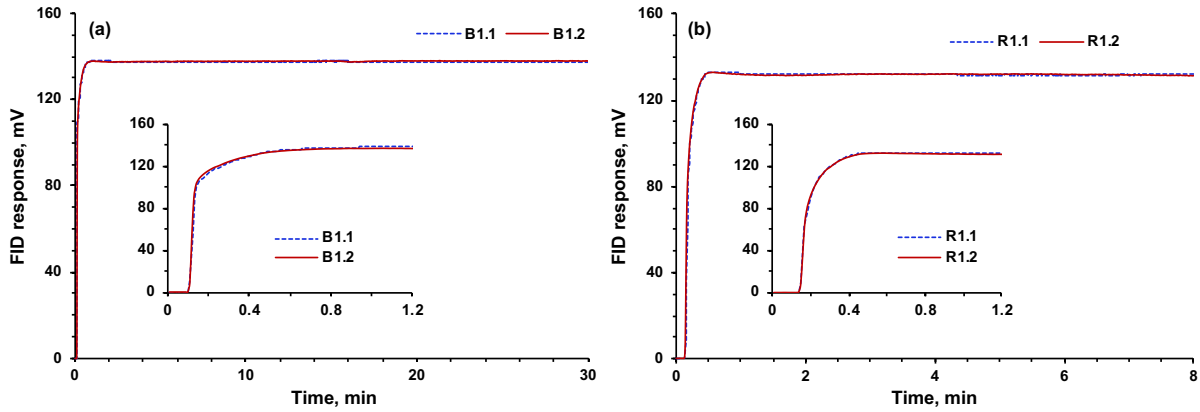

Fig. 2. FID signals recorded in B1.1–B1.2 (a) and R1.1–R1.2 (b). Conditions for the individual tests/runs are available in **Table 2**.

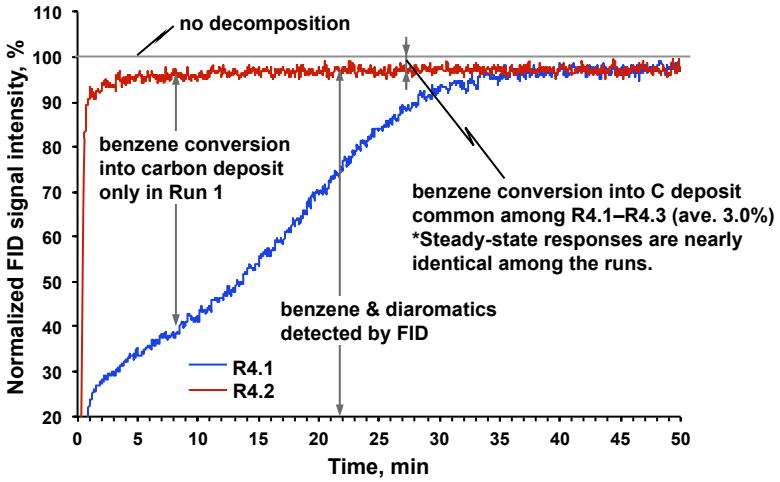

Fig. 3. FID responses in a sequence of two runs R4.1 and R4.2. The signal intensities are normalized by that with no benzene conversion.

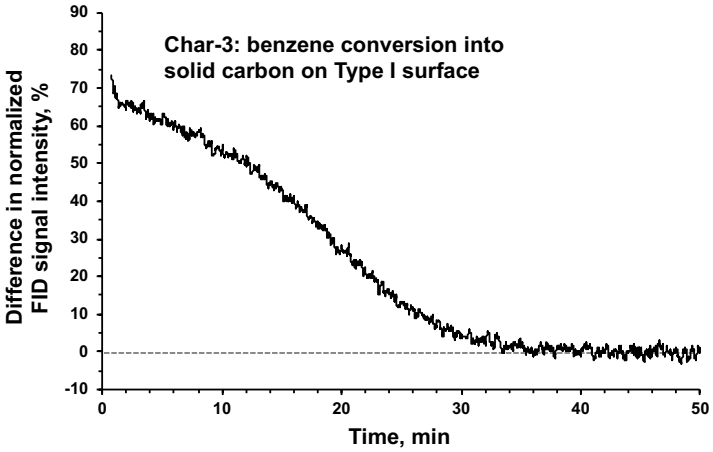

Fig. 4. Difference in the FID signal intensity between R4.1 and R4.2 corresponding to benzene conversion into carbon deposits on Type I surface of fresh Char-3 in R4.1.

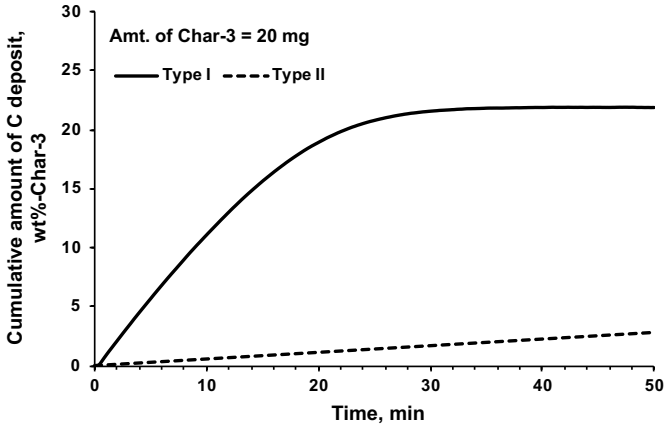

Fig. 5. Cumulative amounts of C deposits onto Type I and Type II surfaces in R4.1. The amount is normalized by the initial mass of Char-3. The amount of C deposit on Type II surface was calculated by assuming a steady conversion of benzene (3.0%) over the period of the sequential R4.1 to R4.3.

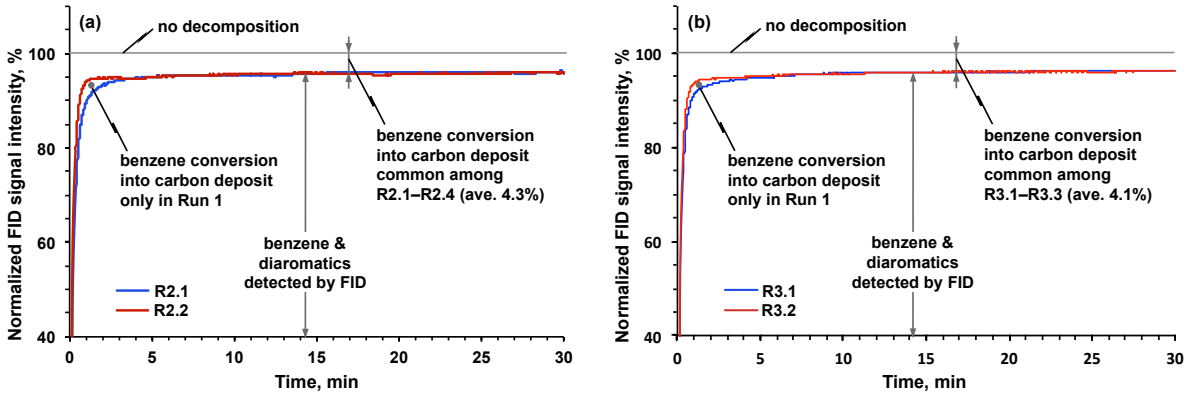

Fig. 6. (a) FID responses in a sequence of two runs R2.1 and R2.2. (b) FID responses in a sequence of two runs R3.1 and R3.2. The signal intensities are normalized by that for no benzene conversion.

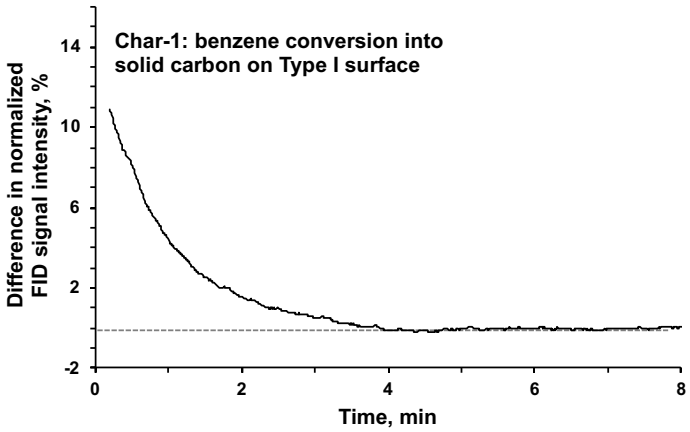

Fig. 7. Difference in the FID signal intensity between R2.1 and R2.2 corresponding to benzene conversion into carbon deposits on Type I surface of fresh Char-1 in R2.1.

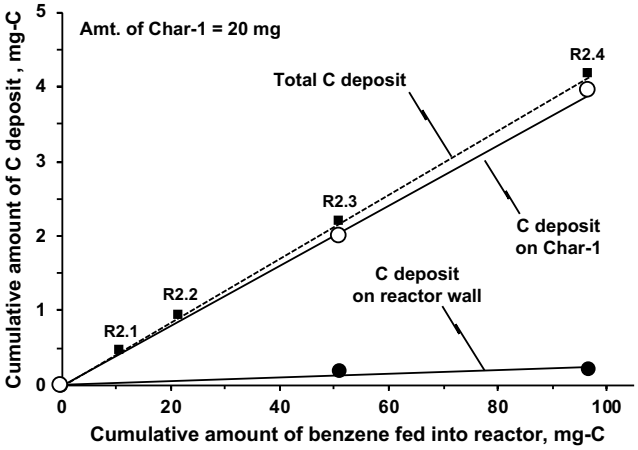

Fig. 8. Relationship between the cumulative amount of benzene fed into the reactor and that of C deposit. Total amount of C deposit (indicated by closed square) does not include that formed on Type I surface (0.036 mg-C, only in R2.1).

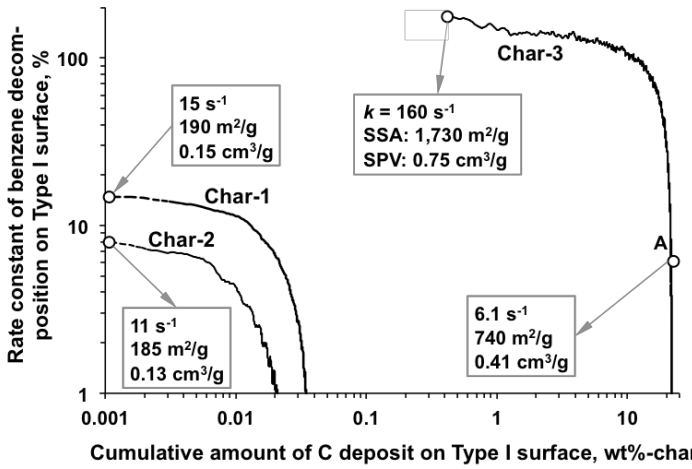

Fig. 9. Changes in the first-order rate constant of benzene decomposition on Type I surface along with C deposition thereon. *k*; first-order rate constant of benzene decomposition on Type I surface, SSA; specific surface area determined by the QS-DFT method, SPV; specific pore volume determined by the QS-DFT method. Point A indicates Char-3 after 30-min exposure to benzene vapor (R4.4).

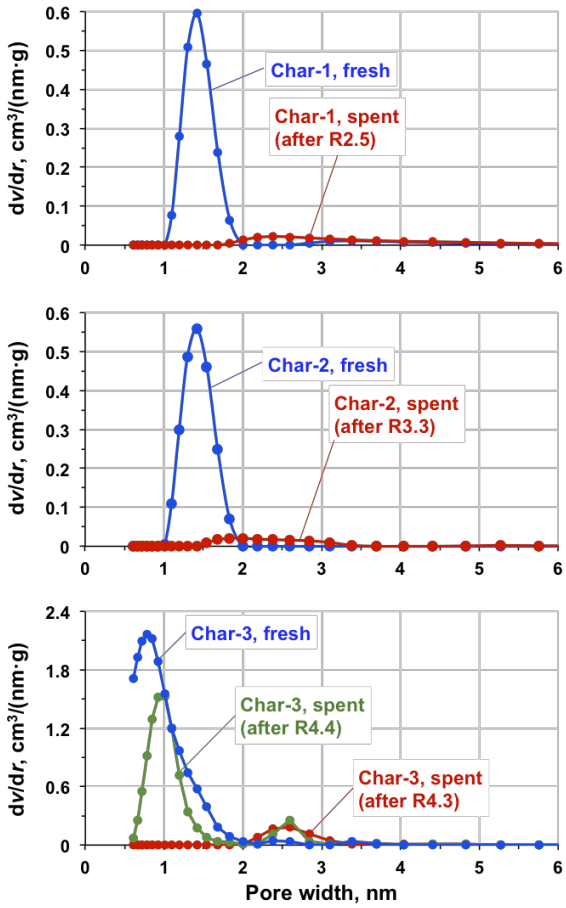

Fig. 10. Pore size distributions for fresh and spent Char-1, Char-2 and Char-3.

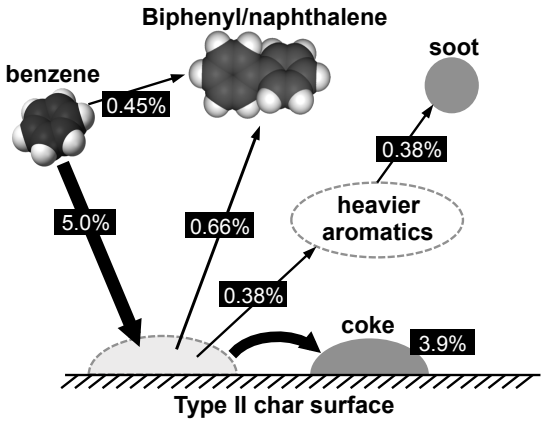

Figure 11. Pathways of benzene conversion on Type II surface. The indicated conversions are based on the results from R2.1 to R2.5.

Chapter 4

Methods for Precise Kinetics Measurement/Analysis of Non-Catalytic and Catalytic CO_2 Gasification of Lignite Char

4.1. Introduction

Char gasification with CO_2 is a slow reaction which is known as the rate-determining step during thermochemical conversion of coal into syngas in a gasifier. Measurement of the gasification rate is important for designing and operating industrial reactors. Rate of gasification has been generally conducted by applying a thermogravimetric analyzer (TGA). Isothermal TGA examining weight loss of sample placed in a crucible draws the rate of the thermochemical conversion with reactive gas at a designated temperature. Successful gas diffusion to internal/external char surface is a presumption for precise measurement of the reaction rate. Experimental conditions such as flow rate, particle size and initial sample loading (i.e., bed thickness) are thus carefully chosen to avoid or minimize inhomogeneous contact between gas and solid. The inhomogeneity is attributed to gas film surrounding particles, which resists gas transport to the outer surface as well as the pores. It was suspected that insufficient flow rate and inappropriate particle size would lead to misinterpretation of kinetics due to char gasification controlled not kinetically but by mass transport.

Effects of external and internal diffusion on CO_2 gasification of char derived from various carbonaceous materials such as biomass and coal using a TGA have been investigated for precise measurement of reaction rates [1-12]. Ollero et al. [1] evaluated diffusional effects on gasification rate of biomass waste by applying two different sizes of crucibles. They also proposed a sample loading near the mouth of a crucible to eliminate limitation of gas transport caused by a stagnant gas layer between the crucible mouth and surface of char bed. Adopting their proposed method, Gómez-Barea et al. [2] investigated intraparticle diffusional effects using different sizes of a single particle of biomass char. They found that reactivity of macroscopic sized char was controlled by the mass transfer limitation

due to increase of internal partial pressure of product CO. Jess and Andresen [3] performed non-isothermal gasification and combustion of cokes, and derived a correlation of external diffusion effects caused by height of crucible applicable to gas-solid reactions. Mani et al. [4] investigated mass transfer limits on gasification of different particle sizes of char derived from wheat straw by confirming effects of temperature and particle size. Similar works were conducted by Huo et al. [5,6] who investigated effects of temperature and particle size on gasification of various ranks of coals and petroleum coke. Kim et al. [7] performed gasification of char derived from Indonesian sub-bituminous coal at elevated temperature and pressure, and correlated empirical data with *n*-th order rate equation adapting internal/external diffusional effects. Geng et al. [8] estimated distribution of CO_2 concentration in stagnant layer during gasification of Chinese lignite by changing the height of crucibles, i.e. the height of stagnant layer, and concentration of CO_2.

Diverse conditions of total gas flow rate and initial weight have however applied to the previous researches. Although appropriate conditions for those variables are dependent on sizes of instrument and a crucible, some of the researches, even including studies investigated the diffusional effects, seemed to have been employed low insufficient flow rate of 100 ml/min or less [4,5,13,14,15]. This was a motivation of the present work. Additionally, most of the previous studies evaluated the external/internal diffusion effects by using Thiele modulus, which is derived from ratio of reaction rate to diffusivity, and/or effectiveness factor, and made efforts to derive a modified rate equation or to model the gas transport phenomena correlating with experimental data. None of the studies were however focused on differences between non-catalytic and catalytic gasification.

Low rank coals, in particular lignite abundantly contains inherent alkali and alkaline earth metallic (AAEM) species that play a catalytic role in char gasification. Such catalytic promotion may lead to mechanism different from that of non-catalytic gasification. It makes difficult to apply well-known gas-solid reaction models such as shrinking core model and random pore model [16] to lignite gasification, particularly when the rate of gasification is close to zeroth order or has a maximum at later stage of conversion [17]. Kinetic models assuming parallel progress of non-catalytic and catalytic gasification have been thus

examined in previous studies [18-21]. Further, no or little diffusional limit of oxidizing agent or product gases on lignite gasification was reported when different particle size of lignite was gasified with steam [22]. Similar results were shown in CO_2 gasification of char derived from sub-bituminous coal varying initial weight and particle size [23]. It was suspected that the contradictory diffusional effect between non-catalytic and catalytic gasification would be arisen from degree of catalytic promotion caused by inherent AAEM species, resulting in difference in gasification mechanism. In the sense, the diffusional effects on catalytic gasification may be distinguishable from that on non-catalytic one, and thus should be examined separately.

This study aims at re-examination of methods for kinetic measurement and analysis considering inter- and intra-particle gas diffusion, which inevitably affects reaction rates in TGA. The present work also focuses on differences of the diffusional effects on catalytic and non-catalytic gasification of lignite with CO_2.

4.2. Experimental

4.2.1. Sample preparation

Victorian lignite, Loy Yang (LY) of which the elemental composition of C, H, N and O+S (by difference) was respectively 66.9, 4.8, 0.6 and 27 wt% on a dry basis, was used for kinetic analysis. Char was prepared from LY pulverized to sizes of 106 μm or less and pyrolyzed in a horizontal electric furnace at peak temperature of 600 °C under N_2 flow at a rate of 300 ml-stp/min (the unit of flow rate on basis of standard temperature and pressure is hereafter denoted simply as ml/min). The pulverization was performed to avoid unfavorable effects of particle size, which will be described later. A heating rate and holding time were 5 °C/min and 10 min, respectively. Char yield was ca. 44 %, and contents of AAEM species such as Na, K, Mg and Ca were measured, which yielded 0.15, 0.009, 0.013 and 0.097 wt%-char, respectively.

Demineralized LY was prepared by a sequential treatment of 3 M HCl and 3 M HF, denoted hereafter as ALY. LY was firstly immersed in the HCl solution and magnetically

stirred for 20 hours at 60 °C. Then, the same treatment was repeated by using the HF solution. The acid-treatment removed drastic amount of AAEM species from LY. The contents of Na, K, Mg and Ca were 0.00027, 0.00026, 0.00048 and 0.0018 wt%-coal, respectively. Although the values are presented on basis of coal weight, the metallic species was sufficiently removed from the parent coal considering the char yield of ca. 46%. ALY was pyrolyzed in the same way as above.

Different sizes of particle were obtained from following procedures. This was performed mainly for making large size of particle, because the coal particles were inevitably ground to sizes of tens of microns by a magnetic stirrer in the course of the acid-treatment. ALY was then briquetted to a disk having a diameter of 14 mm and a thickness of 5 mm under mechanical pressure of 128 MPa and temperature of 200 °C. Pyrolysis of the briquette was performed at peak temperature of 1000 °C with a heating rate of 5 °C/min under atmospheric N_2 flow. It was followed by crushing and sieving to obtain particles in micron sizes.

4.2.2. Thermogravimetric analysis

Isothermal char gasification was performed in a TGA (Hitachi TG/DTA7200) with a cylindrical furnace tube having an inner diameter of 18.4 mm at atmospheric pressure. Char prepared from the above-described procedures was placed on a platinum crucible with a diameter of 5 mm and a depth of 2.5 mm, and a swipe gas was flowed in a horizontal direction. The char was heated up to 1000 °C with a heating rate of 20 °C/min and holding time of 10 min and then cooled down to 900 °C at a rate of 10 °C/min providing only N_2 flow at a rate of 700 ml/min. The total flow rate was changed, if necessary, to a designated value when the temperature reached 900 °C, since the peak temperature of 1000 °C was much higher than that of pyrolysis. After confirming stabilization of temperature, the N_2 flow was switched to equimolar mixture of CO_2 and N_2.

Char reactivity was analyzed by following equations. Non-catalytic gasification is generally assumed to obey a first-order kinetics:

$$\frac{dX}{dt} = k_{nc}(1 - X) \quad (4\text{-}1)$$

where, X, t and k represent char conversion rate, reaction time and a first-order rate constant, respectively. On the other hand, catalytic gasification obeys zeroth-order kinetics:

$$\frac{dX}{dt} = k_c \quad (4\text{-}2)$$

where, k_c is a zeroth order rate constant. Representative reactivity is taken at conversion (X) of 0.5 for both non-catalytic and catalytic gasification. Although those are rough assumptions, conversion profiles were represented better than shrinking core model and random pore model.

In order to assure minimization of the stagnant layer between the crucible mouth and surface of char bed, the char placing at the mouth of a crucible was also confirmed, as proposed by Ollero et al. [1]. Instead of filling in the inside of the crucible with alumina, the char was placed on the outside bottom slightly pushed inside for stable loading. Although alumina is commonly regarded as an inert material, catalytic effects of the inherent metallic species may be more or less deactivated by formation of aluminates and/or aluminosilicates during further thermal cracking at temperature above 600 °C, similarly to that with silica as described in **Chapter 2**. Indeed, char underwent further thermal cracking losing ca. 10 % of its weight while heated up. Hereafter, the sample loading near the mouth is termed to 'mouth loading', and comparison of the conventional sample loading and the mouth loading is shown in **Fig. 1**. Due to the empty space, sample temperature detected by applying the mouth loading would be inconsistent with that of the conventional method. Consecutive measurement was thus performed under the identical set values for flow rate and temperature. The conventional loading was firstly applied to gasification of LY char to adjust and confirm the experimental conditions, and the mouth loading was then applied. Zeroth order rate constants are compared in **Fig. 2**. Little difference is found between the two methods for char loading with variation of flow rate in the range of 150 to 1000 ml/min. No influence of the stagnant layer is therefore confirmed in the present study.

Use of a contaminated crucible may have an unfavorable catalytic promotion of gasification, which leads to incorrect measurement of reactivity. AAEM species may be stuck

on the crucible surface in forms of metal oxides and/or carbonates. Some of those may be irreversibly deactivated by transforming into silicates and/or aluminates when the crucible is cleaned by gas flame, while the other may have activity during gasification. It was suspected that the remained AAEM species would be activated at the temperature of 900 °C, and catalyze gasification. **Fig. 3** presents changes of dX/dt due to the contamination. LY char with initial weight of ca. 1.3 mg was gasified at a flow rate of 700 ml/min. Use of the one-time-used crucible shows slightly higher dX/dt compared to that of the new one, which means the abundant AAEM species can quickly contaminate a crucible. The six-time-used crucible leads to the clearly higher dX/dt compared to the new one. It was believed that gasification was catalytically promoted. The contaminated crucible was then washed with an acidic mixture of 1 M HF and 1 M HNO_3 at 60 °C, which is a method proposed for digestion of AAEM species in ash [24]. Excellent agreement in the dX/dt is confirmed when the washed crucible is used. It is therefore essential to maintain the crucible clean, particularly when the concentration of AAEM species is high in coal/char matrix. All the data are taken from the crucible washed after every single run.

4.3. Results and discussion

4.3.1. Effect of particle size

Five ranges of ALY char particles in micron-sizes were prepared for testing the size effect. Initial loading of 2.5 mg was placed on a crucible, and the above-described conditions were applied for the gasification. **Fig. 4** shows significant changes in the rate of non-catalytic gasification owing to the variance of particle size within micron sizes. The pulverization of particles to smaller sizes increases the gasification rate of ALY char due to increase in total surface area of the bed. It facilitates the contact of CO_2 with active sites exposed from the inside of char. It is concluded that the effect of diffusion is eliminated at particle sizes of 125 μm or smaller. The total surface area, which was believed to fully dominate the progress of gasification, however seems to partly govern the reaction rate, since further pulverization has no influence on the dX/dt when the particles are 38 μm or smaller, showing that the 1–X and dX/dt profiles are nearly identical to each other. Though not shown, it was confirmed that the

specific rate of gasification is unnecessarily proportional to the specific surface area measured by partially gasified LY char at different conversion levels. Detailed examination is out of the scope of this study and will be discussed in future works.

4.3.2. Effect of initial mass

Initial sample mass, in other words, thickness of fixed bed, mostly reflects an influence on gas diffusion within the bed, including a minor effect of pore diffusion. **Fig. 5** shows the mass conversion and dX/dt profiles on non-catalytic gasification measured by varying the initial mass of ALY. Under a fixed total gas flow rate of 700 ml/min, the initial mass was gradually reduced from ca. 3.0 to 1.5 mg on basis of ALY coal mass. It was equivalent to the weight of char bed in the range from 0.6 to 1.2 mg on dry ash-free (d.a.f.) basis. Despite the small changes, the profiles increase with decreasing the initial mass as seen in the figure. The initial mass of 3.0 mg of ALY coal has clearly lower dX/dt values than that of others. The thick bed layer disturbs the penetration of the reactive gas, which causes a gradient of CO_2 partial pressure (or concentration) within the bed. It was empirically expected that the initial char weight of 1.2 mg on d.a.f. basis was sufficiently small to minimize the diffusional limits, however it showed obviously lower reactivity compared to the less amount of initial weight. It was believed that particle agglomeration during the *in situ* pyrolysis would form an inhomogeneous thickness of the char bed, although a monolayer of sample bed is theoretically favored for uniform contact between gas and particles. The increases of the dX/dt became less significant when ALY coal less than 2.0 mg (equivalent to 0.8 mg of char on d.a.f. basis) was initially loaded. Further slight increases were attributed to the less-agglomerated char bed as the initial weight decreased. The peak point in the case of 1.5 mg loading is higher than that of the 2.0 mg loading, however the dX/dt curves become identical to each other at later stage of gasification. The brittle agglomerates are spread as individual particles are shrunk by gasification. It is believed that the bed finally is formed a thin enough, and the gradient of CO_2 partial pressure becomes uniform.

Effect of initial mass on catalytic gasification was also confirmed. LY char of 0.8 to 5.1 mg was gasified under the same conditions as above, and the results are shown in **Fig. 6**.

The dX/dt profiles of the initial mass of 0.8 (0.6 mg-d.a.f.) and 1.3 mg (1.0 mg-d.a.f.) are in excellent agreement in contrast to the non-catalytic gasification in the similar range of variances. The diffusional effects on the catalytic gasification seem much less than that of the non-catalytic one. The dX/dt is nearly constant up to the conversion of 0.6, while it decreases slightly at the later stage. Such decrease would be because of deactivation of the catalysts and/or poor contact between catalysts and free active sites as the surrounding sites are gasified. Besides, it would be also partly attributed to loss of AAEM species retained in the char bed as the bed thickness becomes thin. Metallic species are dissociated by its volatilization during gasification, but the catalytic activity is maintained by associative re-adsorption of volatilized metallic species onto carbon matrix when the bed is sufficiently thick (up to X=0.6). As the bed becomes thin, the volatilized AAEM species are released out of the bed. In case of the initial weight of 5.1 mg (4.0 mg-d.a.f.), such reactivity decrease is negligible, because the bed (1.6 mg-d.a.f. at X=0.6) is still thick enough to prevent the poor contact and loss of AAEM species.

At further increases of the initial mass, the dX/dt profiles are slightly lower than that of the bed loaded 1.3 mg between the beginning and the conversion of 0.6. The dX/dt, i.e. rate of gasification, decreases slightly but systematically with increasing the initial mass of char loading. Similarly to the non-catalytic gasification, such change is attributed to the partial pressure of CO_2 within the bed due to resistance to gas diffusion, in other words, dilution of CO_2 concentration surrounding char particles. The increases of dX/dt at the later stage of gasification (X>0.6) for the initial mass of 2.3 and 5.1 mg are attributed to concentration of AAEM species due to shrinkage of particles. The changes of dX/dt on catalytic gasification are much smaller than that of non-catalytic ones. **Fig. 7** shows comparison of relative representative reactivities (dX/dt at X=0.5), representing ratios of the dX/dt against that of the cases of 0.6 mg (on d.a.f. basis) in each set. It is clear that the non-catalytic gasification is more affected by the diffusional effects than the catalytic one in the same ranges of variances of both flow rate and initial weight. If the resistance of gas diffusion is a main reason for the changes in the reaction rate, it should have more influences on the catalytic gasification rather

than the non-catalytic one. It was suspected that mechanism of the catalytic gasification would differ from the non-catalytic one due to the presence of catalysts.

4.3.3. Effect of flow rate

Both inter- and intra-particle diffusions are strongly related to total gas flow rate. LY and ALY char of 1.3 mg was gasified by varying total gas flow rate in the range from 150 to 1000 ml/min. **Fig. 8** presents the changes of the dX/dt at different flow rates. The non-catalytic gasification rate clearly increases with increasing the total gas flow rate. The near-linear decreases of dX/dt at X>0.2, indicate that the non-catalytic gasification obeys the first order kinetics. The well-known kinetic models such as shrinking core model and random pore model are hard to represent the dX/dt profiles. On the other hand, the catalytic gasification rate hardly changes with the total gas flow rate. The dX/dt curves are larger by an order of magnitude and nearly constant. It indicates that the gasification of LY char is highly dominated by the catalytic promotion, and deactivation of catalysts hardly takes place during the entire range of conversion. Slight change would be attributed to the loss of AAEM species as described above. Similarly, the catalytic gasification obeys the zeroth order kinetics.

Further analysis was performed for better comparison by taking the first and zeroth order rate constants from non-catalytic and catalytic gasification, respectively. **Fig. 9** shows linear relationships between the rate constants and flow rates regardless of the presence of AAEM species. It is believed that the high flow rate reduces resistance of mass transfer between the bulk gas and solid surface. In gas-solid diffusion theory, a gas film, a gaseous layer surrounding a particle is formed and disturbs a flow to the particle, and vice versa. A large flow rate, or gas velocity, is a driving force for making the layer thin. Increase of gas concentration in the layer then facilitates mass transfer at the boundary. In CO_2 gasification, product CO is known as an inhibitor. Contact of product CO with the char surface reduces the rate of gasification. Higher flow rates enable to prevent from the CO inhibition, and it thus leads to the increase of dX/dt.

The total gas flow rate however has much less influences on the catalytic gasification. It is speculated that the CO inhibition is excluded from the catalytic gasification. Net catalytic activity, presented in the zeroth order rate constant, is calculated by subtracting the rate of non-catalytic gasification from that of catalytic one, as shown in **Fig. 10**. The catalytic effect is unaffected by the increase of flow rate up to 1000 ml/min. In other words, the slight changes of the d*X*/d*t* are derived solely from the non-catalytic gasification. Moreover, it is evidence of parallel progress of the non-catalytic and catalytic gasification with no competition, and thus the precise kinetic measurement and analysis of char gasification should be individually conducted. Although it is difficult to derive direct relationship between the content of AAEM species and the rate of gasification, the mechanism can be distinguished from each other, as will be discussed below in detail.

4.3.4. Mechanism of non-catalytic and catalytic gasification

The rate of non-catalytic gasification was affected sensitively by physical diffusion despite very low reactivity with CO_2. The changes of d*X*/d*t* are regarded as a qualitative measure of product gases (mainly, CO) released out of the pores/char bed, because CO is ~~a species known as~~ an inhibitor of gasification. Although mechanism of CO inhibition is not fully understood, it is possibly explained by following descriptions. Firstly, adsorption-desorption mechanism is generally accepted for CO_2 gasification of char as below [25].

$$C_f + CO_2 \rightarrow CO + C(O) \tag{4-2}$$

$$CO + C(O) \rightarrow C_f + CO_2 \tag{4-3}$$

$$C(O) \rightarrow CO + C_f \tag{4-4}$$

where, C_f and $C(O)$ are free active sites and carbon-oxygen complexes, respectively. The rate is expressed as a Langmuir-Hinshelwood (L-H) type equation as follow:

$$r = \frac{k_1 p_{CO_2}}{\frac{k_1}{k_3} p_{CO_2} + \frac{k_2}{k_3} p_{CO} + 1} \tag{4-5}$$

where, k_1, k_2, k_3 and p_n represent the rate constants for eqs. 4-2 to 4-4 and partial pressure of CO/CO_2, respectively. Assuming steady-state condition and quasi equilibrium of carbon oxidation, the L-H rate equation can be simplified,

$$r = \frac{k_3}{\left(\frac{k_2}{k_1}\right)\left(\frac{p_{CO}}{p_{CO_2}}\right)+1} \tag{4-6}$$

It implies that the gasification rate is dominated by not individual partial pressure but ratio of CO and CO_2. The gasification rate is affected by local partial pressure of CO at particle surroundings. Desorption of oxygen from carbon-oxygen complexes (eq. 4-2) is promoted as gasification is progressed. The increase of stagnant CO in the bed/pores inhibits the overall gasification rate. Ollero et al. [26] also showed that the L-H type kinetics well predicted the rate in the presence of CO. Moreover, CO can be chemically adsorbed onto the retained metal ions or metal oxides [27], although only traces of AAEM species were remained after the acid-treatment. It is believed that such affinity facilitates the stagnancy of CO in the char bed, and reduces the reactivity.

On the other hand, no effect of flow rate up to 1000 ml/min was found in the catalytic gasification, although local partial pressure of CO is larger than that of the non-catalytic one due to rapid conversion. It implies that no CO inhibition is involved in the catalytic gasification. The decreases in the dX/dt with large initial mass are attributed to not CO inhibition but locally low partial pressure of CO_2 within the thick bed. Following carbonate formation-decomposition mechanism is suggested when gasification is catalytically promoted by the inherent metallic species. In the CO_2-rich condition, metal oxides (inherently contained or formed by a reaction with CO_2) can be transformed into metal carbonates, of which backward reaction is also available. The carbonates then react with free active sites of carbon and produces CO. The mechanism can be expressed as following equations.

$$MO + CO_2 \rightarrow MCO_3 \tag{4-5}$$

$$MCO_3 \rightarrow MO + CO_2 \tag{4-6}$$

$$MCO_3 + C_f \rightarrow MO + 2CO \tag{4-7}$$

where, *M* is the AAEM species. Two pathways of carbonate-catalyzed gasification can be considered as follows.

$$MCO_3 + C_f \rightleftarrows MO + C(O) + CO \quad (4\text{-}7.1)$$

$$\text{or } MCO_3 + C_f \rightleftarrows MO + 2C(O) \quad (4\text{-}7.2)$$

$$C(O) \rightarrow CO \quad (4\text{-}8)$$

In combination of eq. 4-8 with 4-7.1, CO inhibition affects the rate of gasification through the backward reaction, while no CO inhibition is involved in case of that with eq. 4-7.2. Since no inhibition induced by CO was observed, the latter of mechanism is plausible. Even if CO inhibition is involved, it would be negligibly small compared to the catalytic promotion. L-H type rate equation is hence derived as below.

$$r = \frac{2k_6 C_{C_f} C_{M_t} C_{CO_2}}{C_{CO_2} + \left(\frac{k_5}{k_4} + \frac{k_6}{k_4} C_{C_f}\right)} \quad (4\text{-}9)$$

where, k_4, k_5, k_6 and C_n respectively represent the rate constants for eqs. 4-5 to 4-7 and concentration of n-th species, assuming that total amount of metallic species (M_t) is sum of MO and MCO_3. If the catalyst is always surrounded by sufficient amount of C_f, C_{C_f} can be regarded as a constant, a, then the above equation is

$$r = \frac{2ak_6 C_{M_t} C_{CO_2}}{C_{CO_2} + \left(\frac{k_5}{k_4}\right) + \left(\frac{k_6}{k_4}\right) a} \quad (4\text{-}10)$$

Further, Na and Ca are likely metallic species for the reactions considering its abundance. The gasification is catalyzed by oxide-carbonate cycles as follows.

Oxide-carbonate cycles:

$$Na_2O + CO_2 \rightarrow Na_2CO_3 \quad (\Delta G = -143 \text{ kJ/mol}) \quad (4\text{-}11.1)$$

$$Na_2CO_3 + C \rightarrow Na_2O + 2CO \quad (+109) \quad (4\text{-}11.2)$$

$$CaO + CO_2 \rightarrow CaCO_3 \quad (+10) \quad (4\text{-}12.1)$$

$$CaCO_3 + C \rightarrow CaO + 2CO \quad (-44) \quad (4\text{-}12.2)$$

Each cycle consists of thermodynamically spontaneous and unspontaneous reactions, but the sum of ΔG is negative.

4.4. Conclusions

Methods for kinetic analysis of CO_2 gasification of lignite char were re-evaluated by distinguishing the non-catalytic gasification from the catalytic one. Effects of the total gas flow rate, particle size and initial char mass (in other words, thickness of char bed) on the rate of gasification were investigated by the TGA, and following conclusions were drawn.

(1) The resistance of gas diffusion, which leads to the inhibition of gasification by CO, is minimized at particle size of 125 μm or smaller and initial mass of 1 mg or less.
(2) The rate of gasification increases linearly with increasing the total gas flow rate up to 1000 ml/min regardless of the presence of AAEM species.
(3) The non-catalytic gasification is sensitively affected by the flow rate, while much less effect is found on the catalytic one. Further, the net catalytic activity is unchanged by the flow rate over the range examined, indicating that the CO inhibition is not involved in the catalytic gasification.

References

[1] P. Ollero, A. Serrera, R. Arjona, S. Alcantarilla, Diffusional effects in TGA gasification experiments for kinetic determination, Fuel 81 (2002) 1989–2000.

[2] A. Gómez-Barea, P. Ollero, C. Fernández-Baco, Diffusional Effects in CO_2 Gasification Experiments with Single Biomass Char Particles. 1. Experimental Investigation, Energy Fuels 20 (2006) 2202–2210.

[3] A. Jess, A.-K. Andresen, Influence of mass transfer on thermogravimetric analysis of combustion and gasification reactivity of coke, Fuel 89 (2010) 1541–1548.

[4] T. Mani, N. Mahinpey, P. Murugan, Reaction kinetics and mass transfer studies of biomass char gasification with CO_2, Chemical Engineering Science 66 (2011) 36–41.

[5] W. Huo, Z. Zhou, F. Wang, G. Yu, Mechanism analysis and experimental verification of pore diffusion on coke and coal char gasification with CO_2, Chemical Engineering Journal 244 (2014) 227–233.

[6] W. Huo, Z. Zhou, F. Wang, Y. Wang, G. Yu, Experimental study of pore diffusion effect on char gasification with CO_2 and steam, Fuel 131 (2014) 59–65.

[7] R.-G. Kim, C.-W. Hwang, C.-H. Jeon, Kinetics of coal char gasification with CO_2: Impact of internal/external diffusion at high temperature and elevated pressure, Applied Energy 129 (2014) 299–307.

[8] P. Geng, Y. Zhang, Y. Zheng, Experimental estimate of CO_2 concentration distribution in the stagnant gas layer inside the thermogravimetric analysis (TGA) crucible, Fuel 224 (2018) 250–254.

[9] A. Gómez-Barea, P. Ollero, R. Arjona, Reaction-diffusion model of TGA gasification experiments for estimating diffusional effects, Fuel 84 (2005) 1695–1704.

[10] Q. Song, B. He, Q. Yao, Z. Meng, C. Chen, Influence of Diffusion on Thermogravimetric Analysis of Carbon Black Oxidation, Energy Fuels 20 (2006) 1895–1900.

[11] A. Gomez, N. Mahinpey, Kinetic study of coal steam and CO_2 gasification: A new method to reduce interparticle diffusion, Fuel 148 (2015) 160–167.

[12] C. Wang, Tao Han, Y. Du, Y. Liu, D. Che, Diffusional effects on differences of coal char reactivity between air and oxy-fuel combustion in thermogravimetric experiments, Journal of Thermal Analysis and Calorimetry 125 (2016) 897–904.

[13] W. Zhu, W. Song, W. Lin, Catalytic gasification of char from co-pyrolysis of coal and biomass, Fuel Processing Technology 89 (2008) 890–896.

[14] P. Lahijani, Z. A. Zainal, A. R. Mohamed, M. Mohammadi, CO_2 gasification reactivity of biomass char: Catalytic influence of alkali, alkaline earth and transition metal salts, Bioresource Technology 144 (2013) 288–295.

[15] G. Kovacik A. Chambers B. Özüm, CO_2 gasification kinetics of two alberta coal chars, The Canadian Journal of chemical engineering 69 (1991) 811–815.

[16] S.K. Bhatia, A Random Pore Model for Fluid-Solid Reactions: 1. Isothermal, Kinetic Control, AIChE Journal 26 (1980) 379–386.

[17] Y.Zhang, M.Ashizawa, S.Kajitani, K.Miura, Proposal of a semi-empirical kinetic model to reconcile with gasification reactivity profiles of biomass chars, Fuel 87 (2008) 475–481.

[18] B. Bayarsaikhan, J.-i. Hayashi, T. Shimada, C. Sathe, C.-Z. Li, A. Tsutsumi, T. Chiba, Kinetics of steam gasification of nascent char from rapid pyrolysis of a Victorian brown coal, Fuel 84 (2005) 1612–1621.

[19] T. Kitsuka, B. Bayarsaikhan, N. Sonoyama, S. Hosokai, C.-Z. Li, K. Norinaga, J.-i. Hayashi, Behavior of Inherent Metallic Species as a Crucial Factor for Kinetics of Steam Gasification of Char from Coal Pyrolysis, Energy Fuels 21 (2007) 387–394.

[20] B. Bayarsaikhan, N. Sonoyama, S. Hosokai, T. Shimada, J.-i. Hayashi, C.-Z. Li, T. Chiba, Inhibition of steam gasification of char by volatiles in a fluidized bed under continuous feeding of a brown coal, Fuel 85 (2006) 340–349.

[21] E. Byambajav, Y. Hachiyama, S. Kudo, K. Norinaga, J.-i. Hayashi, Kinetics and Mechanism of CO_2 Gasification of Chars from 11 Mongolian Lignites, Energy Fuels 30 (2016) 1636–1646

[22] M. Kajita, T. Kimura, K. Norinaga, C.-Z. Li, J.-i. Hayashi, Catalytic and Noncatalytic Mechanisms in Steam Gasification of Char from the Pyrolysis of Biomass, Energy Fuels 24 (2010) 108–116.

[23] I. Matsui, D. Kunii, T. Furusawa, Study of char gasification by carbon dioxide. 1. Kinetic study by thermogravimetric analysis. Industrial Engineering Chemistry Research 26 (1987) 91–95.

[24] C.-Z. Li, C. Sathe, J.R. Kershaw, Y. Pang, Fates and roles of alkali and alkaline earth metals during the pyrolysis of a Victorian brown coal, Fuel 79 (2000) 427–438.

[25] S. Ergun, Kinetics of the reaction of carbon dioxide with carbon, Physical Chemistry 60 (1956) 480–485.

[26] P. Ollero, A. Serrera, R. Arjona, S. Alcantarilla, The CO_2 gasification kinetics of olive residue, Biomass and Bioenergy 24 (2003) 151–161.

[27] G. Pacchioni, P. S. Bagus CO Chemisorption on Oxide Surfaces: Bonding and Vibrations. In: G. Pacchioni, P. S. Bagus, F. Parmigiani (eds) Cluster Models for Surface and Bulk Phenomena. NATO ASI Series (Series B: Physics), vol 283. Springer, Boston, MA, 1992.

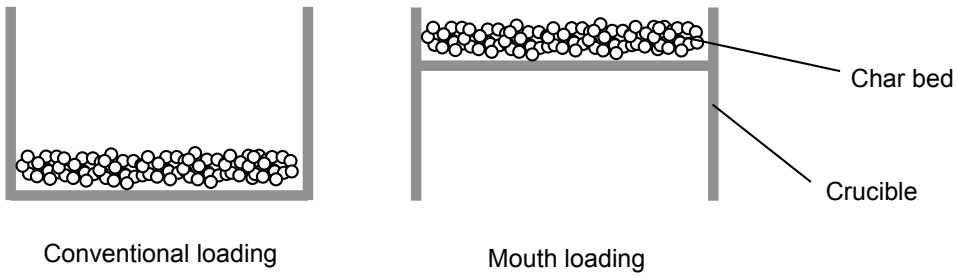

Fig. 1. Sketch of char loading. The ‘mouth-loading’ is tested for comparing effect of stagnant layer between crucible mouth and char bed surface at the conventional loading.

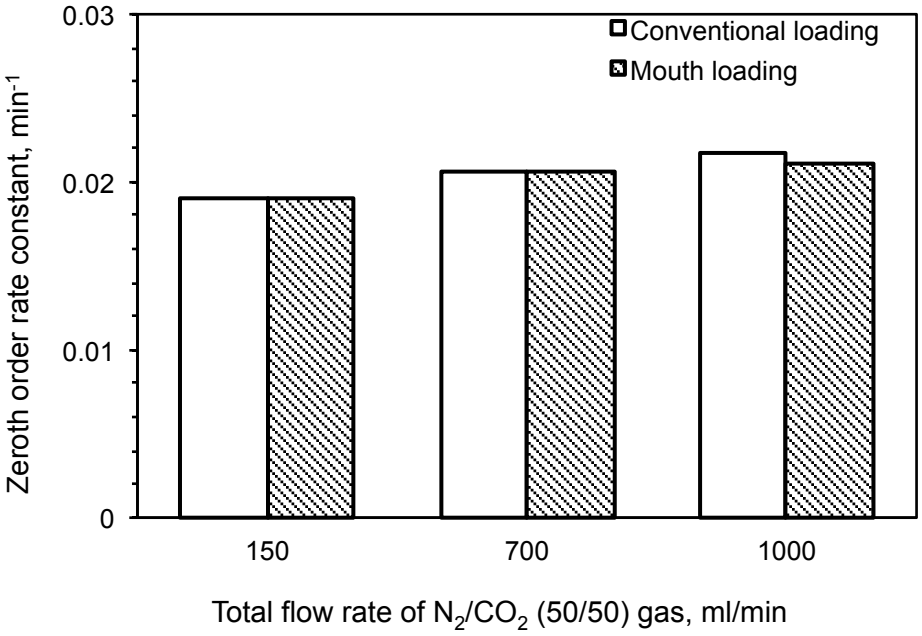

Fig. 2. Comparison of methods of sample loading in terms of zeroth order rate constant

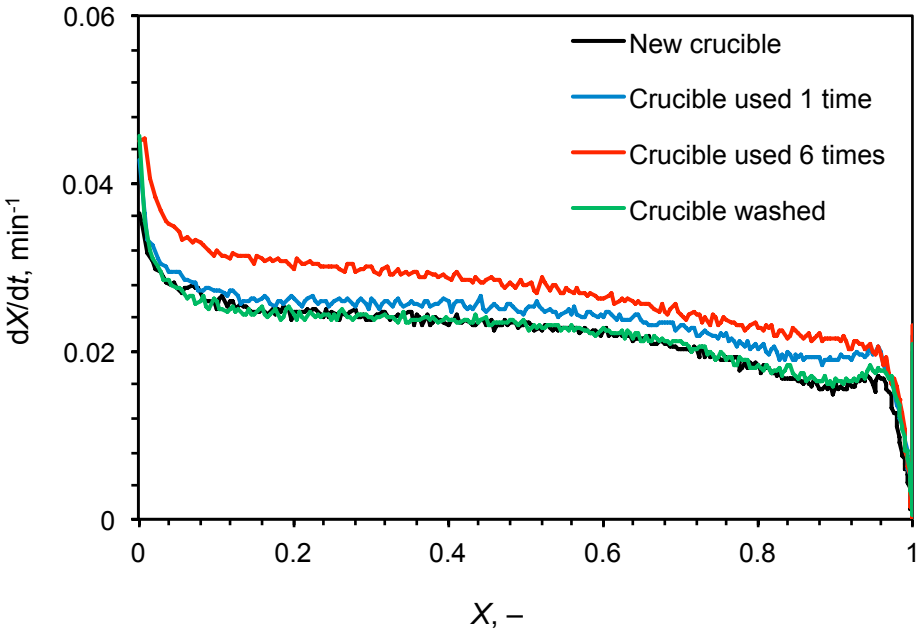

Fig. 3. Comparison of dX/dt vs X profiles of mouth-loaded LY char gasification using new, washed and contaminated crucibles

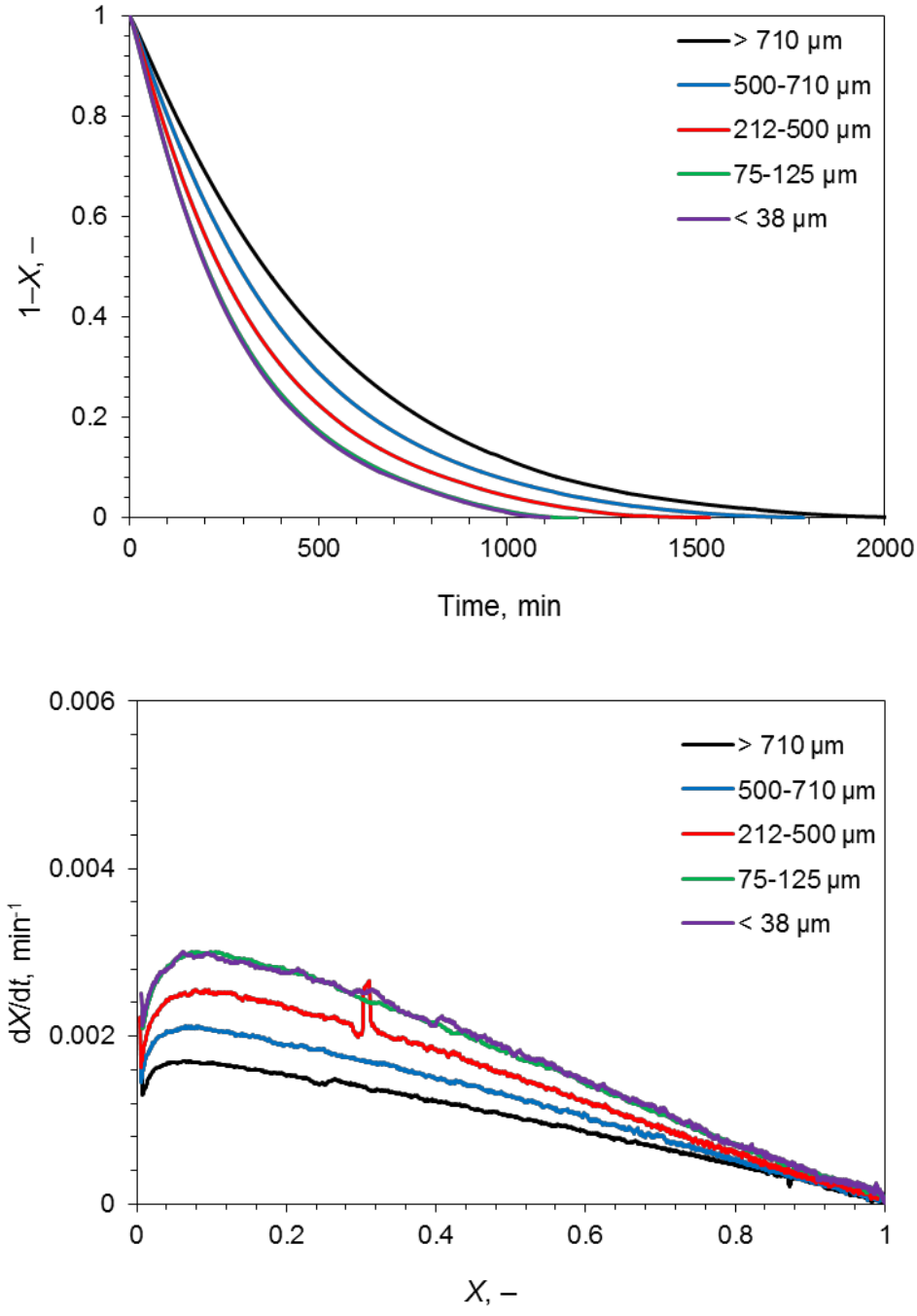

Fig. 4. Profiles of 1–X vs time (top) and dX/dt vs X (bottom) of ALY char gasification varying particle size. 2.5 mg of ALY char is initially loaded and gasified at a flow rate of 700 ml/min.

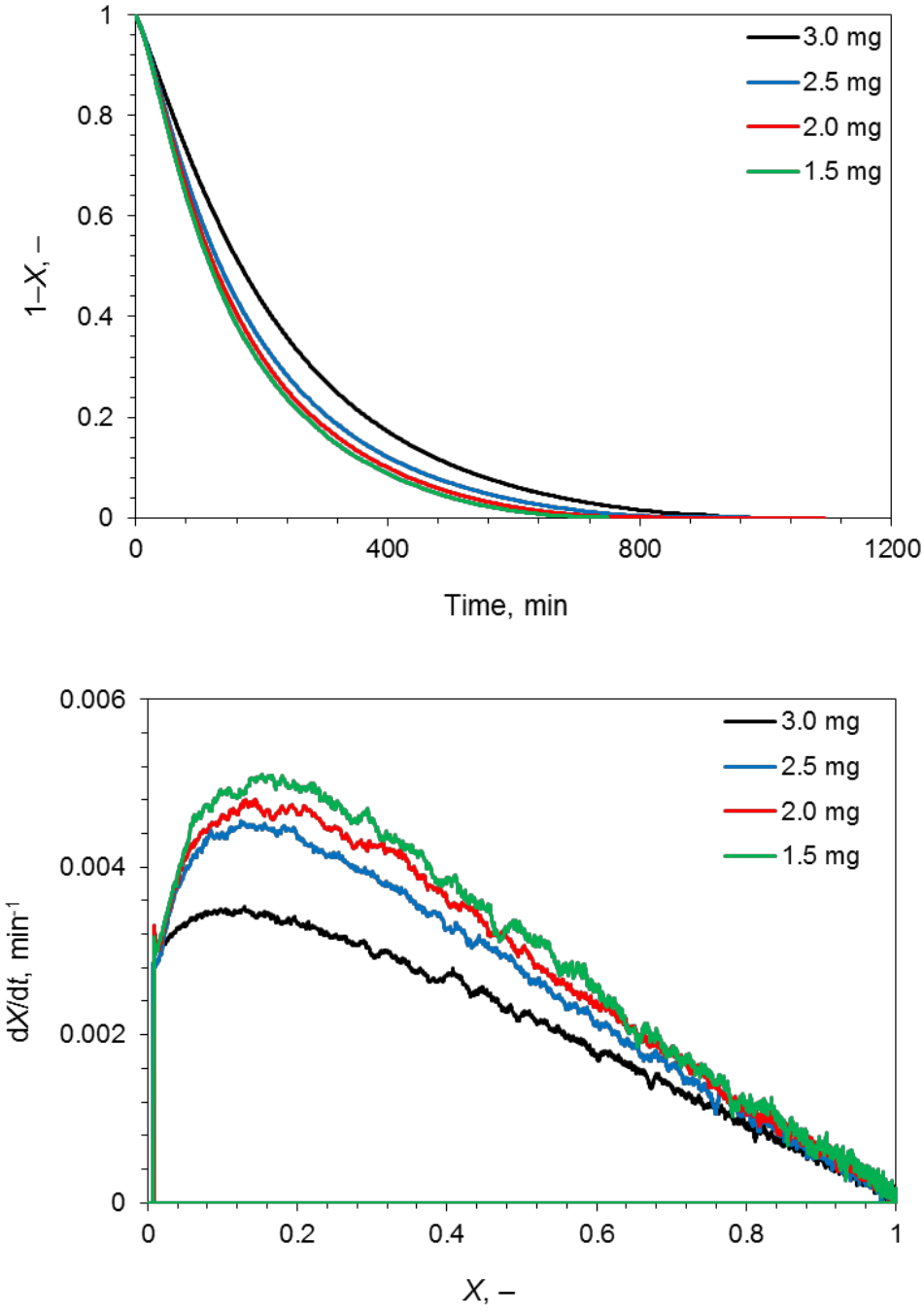

Fig. 5. Profiles of 1–X vs time (top) and dX/dt vs X (bottom) of ALY char gasification varying initial sample weight. The total gas flow rate is 700 ml/min, and the particle size is 106 μm or smaller.

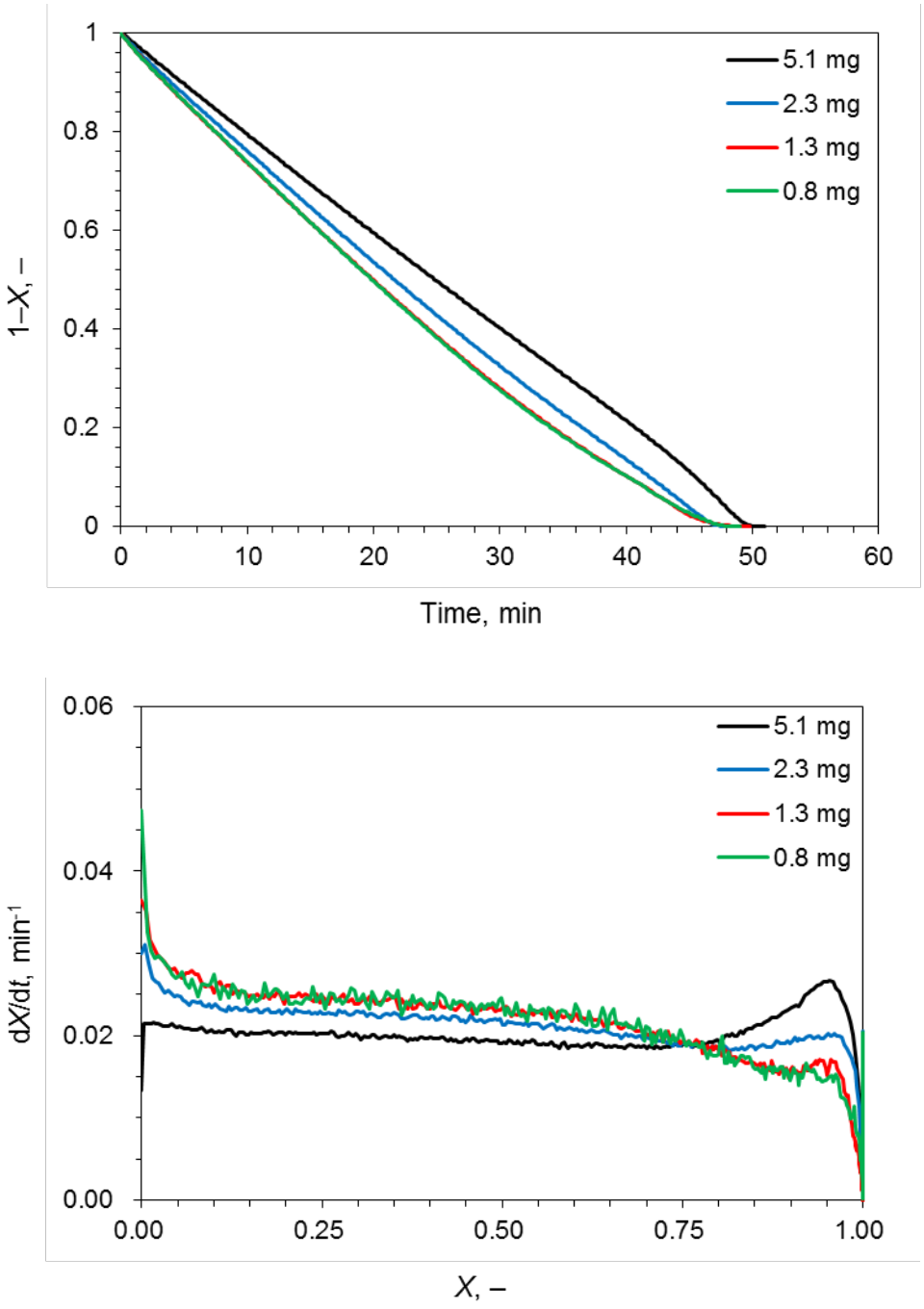

Fig. 6. Profiles of 1–*X* vs time (top) and d*X*/d*t* vs *X* (bottom) of LY char gasification varying initial sample weight. The total gas flow rate is 700 ml/min, and the particle size is 106 μm or smaller.

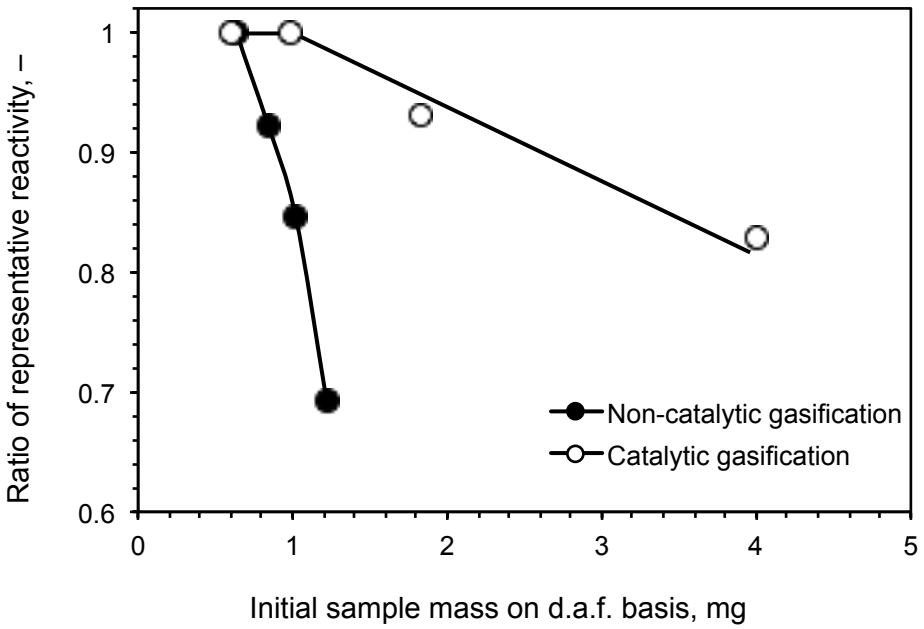

Fig. 7. Changes in the ratio of representative reactivities at X=0.5. The total gas flow rate is 700 ml/min, and the particle size is 106 μm or smaller.

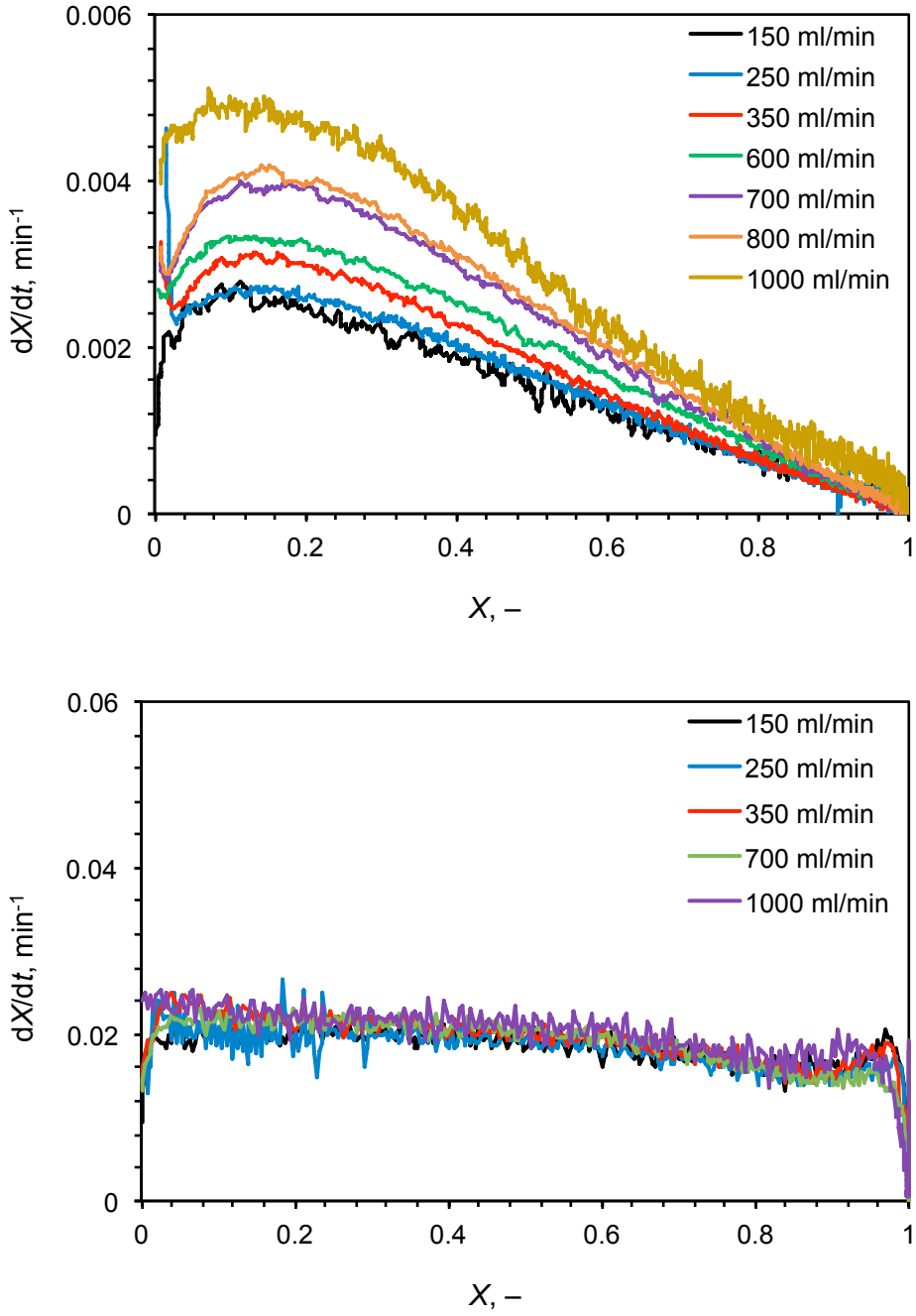

Fig. 8. Profiles dX/dt vs X of ALY (top) and LY (bottom) char gasification at different flow rates. The particle size is 106 μm or smaller, and the initial mass is 1.3 mg.

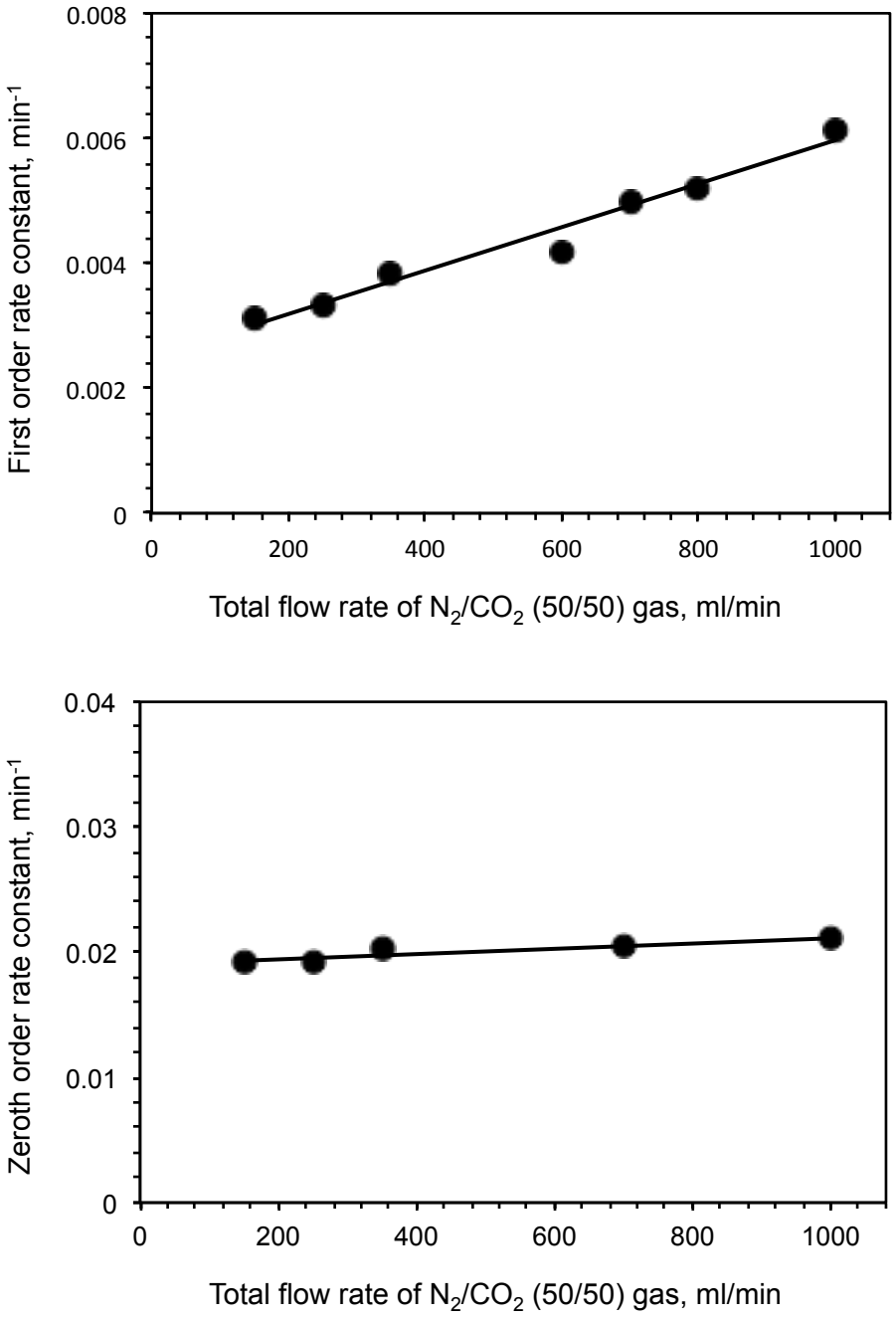

Fig. 9. Profiles of dX/dt vs X of ALY (top) and LY (bottom) char gasification at different flow rates. The particle size is 106 μm or smaller, and the initial mass is 1.3 mg.

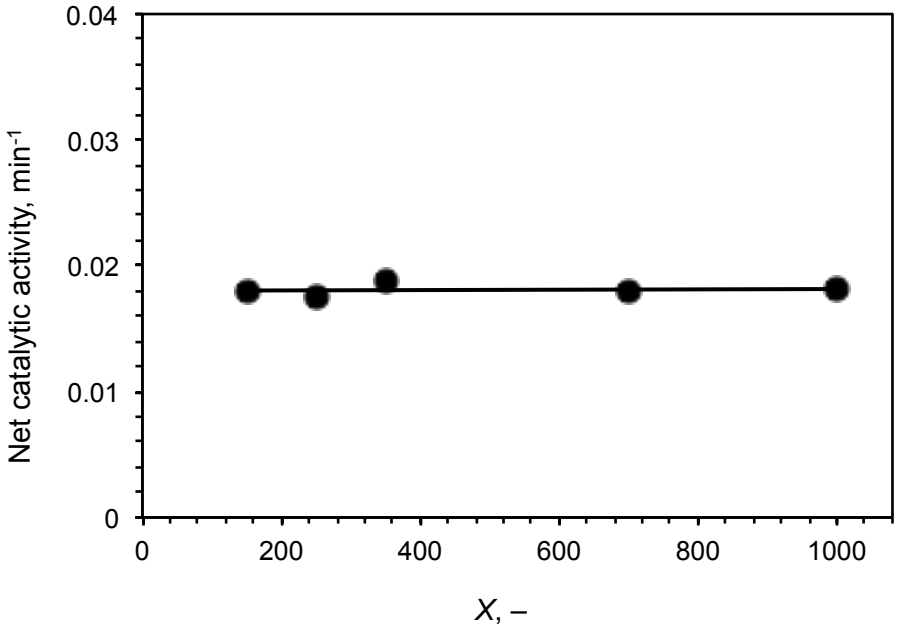

Fig. 10. Net catalytic activity at different flow rates.

Chapter 5

General Conclusions

Low temperature gasification is an important option for future industries due to its flexibility in terms of feedstock and end-use application. It integrates chemical energy from various organic resources with thermal energy into a simple form of product, i.e. syngas, while current gasification technology involves inevitable chemical energy loss due to high operating temperature and large degree of exothermic oxidation. Lignite gasification with CO_2 is proposed as a promising option applicable to the advanced technology due to the features of lignite that has high reactivity arisen from abundant metallic species and activity toward tar vapor caused by large surface area when converted to char. Such features are directly associated with key chemical reactions in low temperature gasification, which are deactivation of catalytic activity induced by inherent minerals and elimination of tar over char surface. As extensive application of the characteristics is encouraged, comprehensive understanding of the phenomena is indispensible to cope with the technical issues. Qualitative understanding of catalytic behavior and tar decomposition in the presence of char has been accumulated, while quantitative examination, particularly precise kinetic analysis, has been insufficient. Therefore, this study aims at investigation of kinetics of the above-described key reactions.

The conclusions of this thesis are summarized as below.

Chapter 2 described mechanism of deactivation of catalytic effect of inherent metallic species in CO_2 gasification of coke from lignite. The inherent catalyst deactivation was experimentally simulated by blending a Victorian lignite with SiO_2, briquetting the SiO_2/lignite blend, carbonizing the briquette, and then gasifying the coke with CO_2. The kinetic analysis of the gasification employed a comprehensive model, which assumed progress in parallel of non-catalytic and catalytic gasification. The model quantitatively described the measured kinetics of the coke gasification with different SiO_2 contents over a

range of coke conversion up to 99.9%. The kinetic analysis revealed that the SiO_2 deactivated substantial and entire portions of the most active catalyst and its precursor, respectively, before the gasification (i.e., during the carbonization). The catalyst deactivation also occurred during the gasification, but mainly following a self-deactivation mechanism that involved no silicates formation.

Chapter 3 proposed a continuous measurement method for decomposition of aromatic vapors on char surface. Kinetics of thermal decomposition of benzene, the most refractory aromatic compound, on lignite-derived char was investigated at 900°C by applying a new method to continuously monitor the char surface activity. Benzene vapor was continuously forced to pass through a micro fixed bed of char with residence time as short as 7.6 ms, and then detected continuously by a flame-ionization detector. Results showed the presence of two different types of char surfaces; consumptive Type I surface and non-consumptive (sustainable) Type II surface. Type I surface of a partially CO_2-gasified char had an capacity of carbon deposit from benzene over 20 wt%-char and an initial activity (represented by a first-order rate constant) as high as 160 s^{-1}. Both of them decreased with increasing carbon deposit due to consumption of micropores accessible to benzene, and finally became zero leaving Type II surface that had a very stable activity with rate constant of 4 s^{-1}. The chars without gasification had capacities of Type I surfaces smaller by two orders of magnitude than the partially gasified char, while the Type II surfaces had activities similar to that of the partially gasified char. It was found that Type II surface converted benzene into not only carbon deposit but also diaromatics and even greater aromatics. Composition of the greater aromatics was unknown because they were deposited onto the reactor wall immediately after passing through the char bed.

Chapter 4 re-evaluated methods for kinetic measurement of catalytic and non-catalytic gasification of lignite char with CO_2 in a thermogravimetric analyzer. Effects of total gas flow rate, particle size and initial char mass (in other words, thickness of char bed) on the rate of gasification were investigated at atmospheric and isothermal conditions. Char derived from lignite and that from demineralization was gasified with CO_2 at 900 °C. It was found that the resistance of gas diffusion, which leads to the inhibition of gasification by CO, was

minimized at particle size of 125 μm or smaller and initial mass of 1 mg or less. The rate of gasification increased linearly with increasing the total gas flow rate up to 1000 ml/min, of which effect on the catalytic gasification was much less than that the non-catalytic one. By subtracting the rate of non-catalytic gasification from that of catalytic one, it was found that the net catalytic activity is constant over the range of flow rate examined. It is evident that the CO inhibition is solely involved in the non-catalytic gasification which is progressed in parallel with the catalytic one with no competition. Mechanism of char gasification in the presence of the catalytic species is therefore suggested.

In conclusion, it can be said that this work quantitatively identified and verified chemical reactions possibly taken place in low temperature gasification and contributed to successful development of advanced gasification technology such as co-production of power and chemicals integrated with solid oxide fuel cell.

Acknowledgements

This thesis would not have been successfully completed without huge supports and contributions from many people to whom I would like to express my sincere appreciation.

I would like to show my greatest appreciation to my supervisor, Prof. Jun-ichiro Hayashi for his excellent supervision and enthusiastic discussion throughout my studies at Kyushu University. His immense knowledge, passion and vision inspired me to be a better researcher and to continue my career in the field of chemical engineering. His constant friendly support has been invaluable for my work and my life in the past four years. With out his support and persistent help, this thesis would not have materialized.

I am grateful to Associate Prof. Shinji Kudo who gave me constructive comments and warm encouragement. His kind guidance and advice on my work helped me to improve its quality, and discussion with him has been always illuminating.

I appreciate the feedback offered by the members of the examination committee, namely Associate Prof. Shinji Kudo, Prof. Jun-ichiro Hayashi and Prof. Hisahiro Einaga. Their insightful comments and suggestions helped me to make this work complete.

I would like to offer my special thanks to Prof. Koyo Norinaga for his constant encouragement and suggestion. His expertise stimulated my interest in the numerical simulation of chemical reactions and broadened my academic knowledge.

I have received generous support from Dr. Xiangpeng Gao who offered the internship at Murdoch University, Australia. His fruitful discussion and guidance showed me new directions in my work.

I would like to acknowledge the Kyushu University Program for Leading Graduate School: Global Strategy for Green Asia for the financial support.

I am deeply indebted to the members in Hayashi/Kudo laboratory, Prof. Seong-Ho Yoon, Mr. Dong-Yeon Ryu and Mr. Sung-Jin Kim for their sincere support.

Last but not least, I wish to thank to my beloved family for their patience and continuous encouragement throughout the course of this study.